iScience

CellPress
OPEN ACCESS

Article

Impact of liver-specific GLUT8 silencing on fructose-induced inflammation and omega oxidation

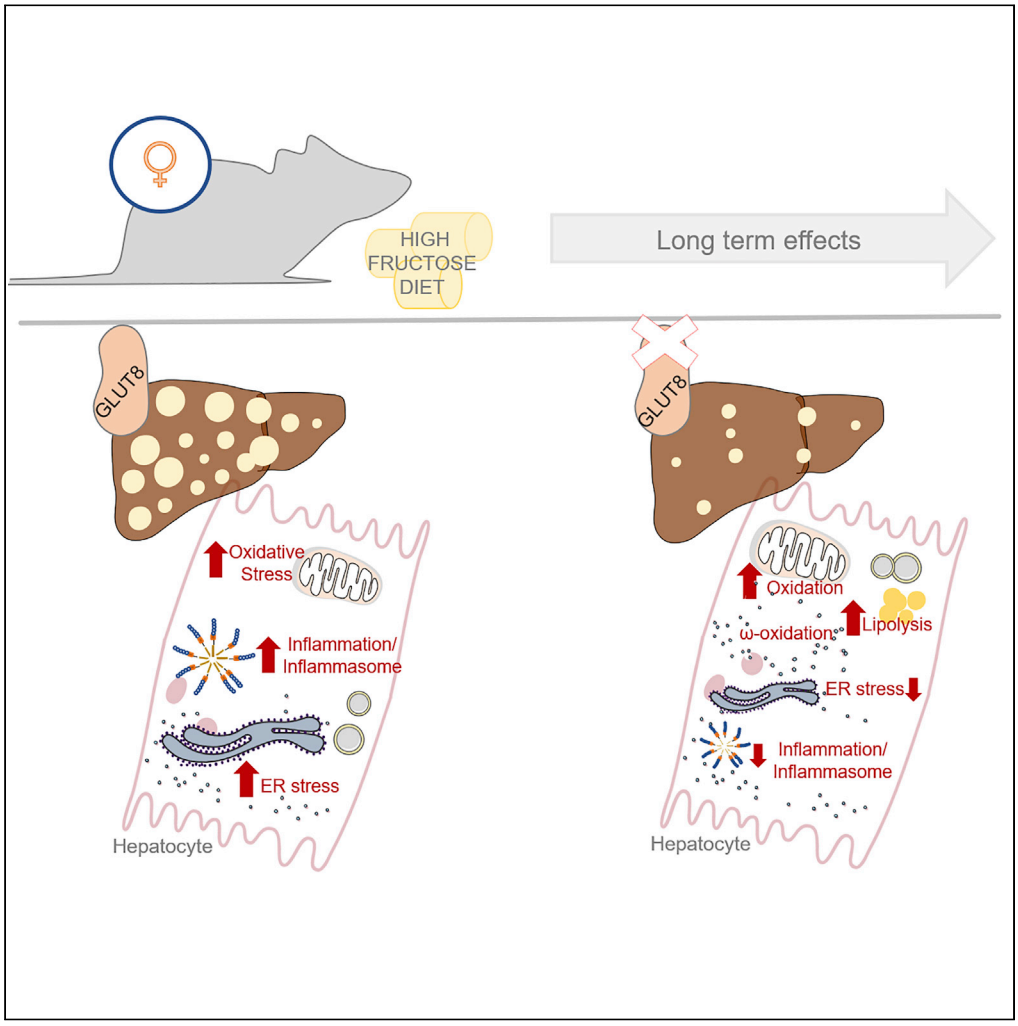

Marta G. Novelle, Susana Belén Bravo, Maxime Deshons, ..., Manuel Alejandro Fernández-Rojo, Carlos Diéguez, Amparo Romero-Picó

carlos.dieguez@usc.es (C.D.)
amparo.romero@usc.es (A.R.-P.)

HIGHLIGHTS

Liver injury induced by high-fat or fructose diet occurs through different mechanisms

Fructose increases inflammatory responses and activates pathological ER stress

Liver-specific GLUT8 knockdown ameliorates fructose-induced injury

GLUT8 knockdown increased lipid mobilization partially driven by omega oxidation

Novelle et al., iScience 24, 102071
February 19, 2021
https://doi.org/10.1016/j.isci.2021.102071

iScience

CellPress
OPEN ACCESS

Article

Impact of liver-specific GLUT8 silencing on fructose-induced inflammation and omega oxidation

Marta G. Novelle,[1,5] Susana Belén Bravo,[2] Maxime Deshons,[3] Cristina Iglesias,[1] María García-Vence,[2] Rebecca Annells,[4] Natália da Silva Lima,[1] Rubén Nogueiras,[1] Manuel Alejandro Fernández-Rojo,[5,6] Carlos Diéguez,[1,*] and Amparo Romero-Picó[1,7,*]

SUMMARY

Excessive consumption of high-fructose diets is associated with insulin resistance, obesity, and non-alcoholic fatty liver disease (NAFLD). However, fructose differentially affects hepatic regulation of lipogenesis in males and females. Hence, additional studies are necessary in order to find strategies taking gender disparities in fructose-induced liver damage into consideration. Although the eighth member of facilitated glucose transporters (GLUT8) has been linked to fructose-induced macrosteatosis in female mice, its contribution to the inflammatory state of NAFLD remains to be elucidated. Combining pharmacological, biochemical, and proteomic approaches, we evaluated the preventive effect of targeted liver GLUT8 silencing on liver injury in a mice female fructose-induced non-alcoholic steatohepatitis female mouse model. Liver GLUT8-knockdown attenuated fructose-induced ER stress, recovered liver inflammation, and dramatically reduced fatty acid content, in part, via the omega oxidation. Therefore, this study links GLUT8 with liver inflammatory response and suggests GLUT8 as a potential target for the prevention of NAFLD.

INTRODUCTION

Non-alcoholic fatty liver disease (NAFLD) constitutes a global public health concern since it is the fastest-growing cause of end-stage liver disease and hepatocellular carcinoma (HCC). The prevalence of NAFLD parallels that of obesity and metabolic syndrome and is expected to continue rising over the next few years. One of the reasons for the increase in liver disease is related to a significant augment in the consumption of diets enriched in sugars, such as fructose which is a major component of the most widely used sweeteners in the western world, especially in beverages (Jensen et al., 2018; Vos and Lavine, 2013). Data gleaned over the last few years have allowed uncovering some of the mechanisms related to NAFLD development and associated comorbidities to be discovered. In this context, animals fed with high fructose diets have emerged as an important dietary model alongside high-fat/cholesterol or the methionine and choline-deficient diets (Lau et al., 2017; Van Herck et al., 2017; Zhong et al., 2020). Indeed, fructose intake has been proposed as a key player in the development of fatty liver disease (Basaranoglu et al., 2013; Hannou et al., 2018; Jegatheesan and De Bandt, 2017). Hence, a better understanding of liver fructose metabolism will facilitate the design of novel pharmacological therapies for NAFLD.

On the other hand, it is generally accepted that mechanisms involved in the development of liver disease are determined by the existence of sex differences. Both basic animal models and clinical studies have reported that males present higher severity and risk of NAFLD than female, at least during the reproductive stage (DiStefano, 2020b; Du et al., 2017; Lonardo et al., 2019). This sexual dimorphism has a crucial role in the onset, progression and treatment response of NAFLD. In fact, male mice fed long-term on high-fat diet (HFD) display steatohepatitis and inflammasome activation, whereas female mice have steatosis without inflammation (Ganz et al., 2014). In general, in animal NALFD models, male subjects present more severe steatosis and steatohepatitis, more pro-inflammatory/profibrotic cytokines, and a higher incidence of hepatic tumors than females. Contrastingly, it has also been reported that female mice develop more severe steatosis than males when fed a cafeteria diet (Gasparin et al., 2018). These apparent discrepancies could

[1]Functional Obeosomics and Molecular Metabolism laboratories, Centro singular de Investigación en Medicina Molecular y Enfermedades Crónicas (CiMUS), Universidad de Santiago de Compostela, CIBER Fisiopatología de la Obesidad y Nutrición (CIBERobn), Instituto de Salud Carlos III, Av. Barcelona s/n 15782, A Coruña, Santiago de Compostela, Spain

[2]Proteomic Unit, Health Research Institute of Santiago de Compostela (IDIS), 15706 Santiago de Compostela, Spain

[3]Laboratoire de Toxicologie, Faculté de Pharmacie, Université Clermont Auvergne, 63000, Clermont-Ferrand, France

[4]Department of Physiology, Anatomy and Genetics, University of Oxford, OX1 3PT, Oxford, UK

[5]Hepatic Regenerative Medicine Laboratory, Madrid Institute for Advanced Studies (IMDEA) in Food, CEI UAM+CSIC, Madrid, E28049, Spain

[6]School of Medicine, The University of Queensland, Herston, 4006, Brisbane, Australia

[7]Lead contact

*Correspondence: carlos.dieguez@usc.es (C.D.), amparo.romero@usc.es (A.R.-P.)

https://doi.org/10.1016/j.isci.2021.102071

be explained by the fact that the liver proteins involved in glucose and lipid metabolism, inflammation or oxidative stress are differentially regulated between sexes. In this context, several studies indicate that this disparity is due to the preventive role of estrogen in hepatic steatosis (Chukijrungroat et al., 2017) among other mechanisms. Accordingly, recent studies have showed that higher hepatic estrogen-related receptor α expression in female mice contributes to the sex disparity in the assembly and secretion of hepatic triglyceride (TG)-rich very low-density lipoproteins (Yang et al., 2020).

Interestingly, despite females being at lower risk of NAFLD development when comparing with males (Balakrishnan et al., 2020; Lonardo et al., 2019), rodent data support the idea that this risk can increase when liver damage is mediated by fructose intake (Choi et al., 2017; Hyer et al., 2019; Spruss et al., 2012). Accordingly, human studies also revealed that women could be more affected than men by the ingestion of higher amounts of fructose than men and a fructose-rich diet sustained over time may lead to changes in hepatic fatty acid (FA) portioning and eventually to increased liver fat content (DiStefano, 2020a; Kang and Kim, 2017; Low et al., 2018; Rodgers et al., 2019). In line with this, studies in rats indicate that these sex differences were related to the fact that the liver enzyme fructokinase, which controlls fructose metabolism in the liver, was markedly induced by fructose liquid ingestion in females but not in males (Vila et al., 2011). In contrast to the large amount of data reporting the effect of high-fructose diet in male animals, the study of the impact of elevated consumption of fructose t in females has been neglected.

GLUT8 (Slc2A8) is the eighth member of facilitated hexose transporters superfamily. Despite knowledge about the tissue distribution and subcellular localization of GLUT8, its complete physiological function remains obscure. It has been shown that global GLUT8-deficient female mice present impaired hepatic first-pass fructose metabolism and, therefore, are protected from fructose-induced macrosteatosis (Debosch et al., 2014); however, its contribution to the physiopathology of NAFLD development is poorly understood. In this study, we examine in-depth two preclinical models of diet-induced NAFLD-non-alcoholic steatohepatitis (NASH) in female: one based on high-fructose and the other based on high-fat, to allow direct comparisons. Specifically, we addressed in female mice the following questions: (1) how detrimental is a fructose-enriched-diet and its impact in terms of deregulation of lipid metabolism, ER stress, oxidative stress and inflammation; (2) the impact of specific GLUT8 silencing on these parameters; and (3) the potential role of GLUT8 in the response to fructose-intake in hepatocytes (HCs) and liver stellate cells.

Our data show that long-term high-fructose intake is associated with NAFLD-NASH development in the absence of increased adiposity and/or obesity. This includes classical features of liver disease, such as liver fat deposition, lipotoxicity, and inflammation. Whole quantitative proteomic analysis and pathway enrichment showed a similarity with some of the known features of human liver disease. This adds further support to the translational value of our data, showing the prevention of NASH in animals with genetic silencing of liver GLUT8.

RESULTS

High fructose and high fat promote different patterns of fatty liver

In contrast to HFD, animals exposed to prolonged exposure to a high-fructose diet showed similar body weight and adiposity to control animals under standard chow (Figures S1 and S2). Liver weight was increased in the high-fructose diet at all time points in comparison to control animals (Figure 1A). Following 22 weeks of exposure to either, HFD or high-fructose diet, there was a marked increase in liver fat accumulation (Figures 1B and 1C), and TG liver content (Figure 1D) as well as in cholesterol serum levels (Figure 1E) while levels of non-esterified fatty acids (NEFAs) levels were unaffected with the exception of elevated NEFAs in 12 week-HFD females (Figure 1D). Assessment of glucose homeostasis following GTT showed, as expected, insulin resistance in HFD animals and normal responses to insulin in high-fructose diets (Figure S3).

Animals exposed to high-fructose diet exhibited increased protein levels of lipogenic enzymes such as fatty acid synthase (FAS) and acetyl-CoA carboxylase (ACC) (Figure 1F), while protein levels of enzymes involved in lipid mobilization like adipose triglyceride lipase (ATGL) and carnitine palmitoyltransferase 1A (CPT1A) were reduced after 22 weeks fructose ingestion (Figure S4C). Gene expression of elongation of very-long-chain fatty acids (VLCFAs) protein 6 (Elovl6) and the endoplasmic reticulum enzyme stearoyl-CoA desaturase (Scd1) were differently regulated after 22 weeks of fructose consumption (Figure S4B). Overall, these

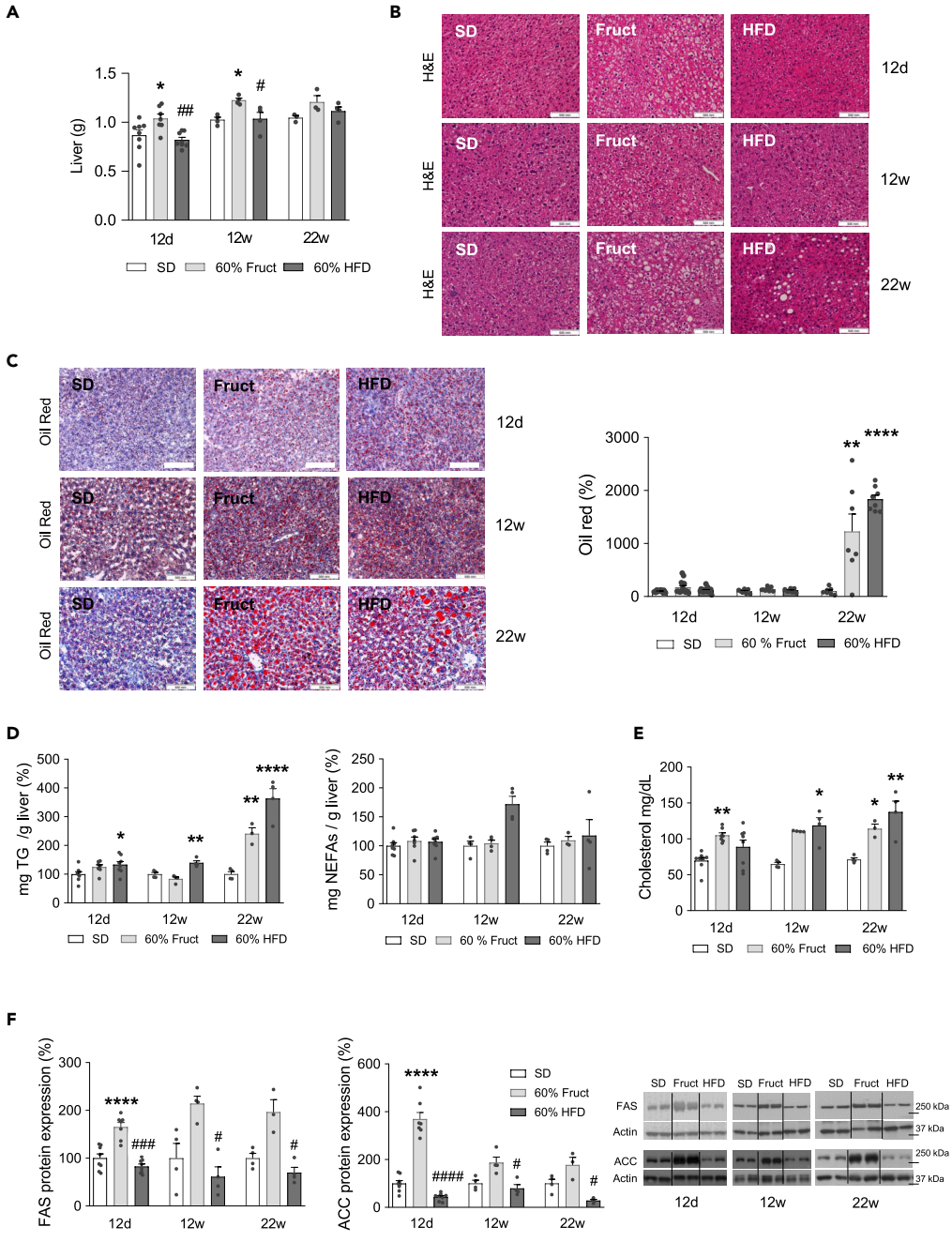

Figure 1. High-fructose and high-fat diets promote fatty liver accumulation in a different pattern

C57BL/6 female mice were fed with Standard Diet (SD), high-fructose (60% Fruct) or high-fat diet (60% HFD). Twelve days (n = 8 per group), 12 weeks (n = 4 per group), and 22 weeks (n = 3–4 per group) post-feeding, livers were isolated, (A) weighed, and subjected to (B) hematoxylin and eosin (H&E) (Scale bar: 50 μm). Total liver FA was measured by (C) Oil Red dyeing (Scale bar: 50 μm), and (D) the liver content of triglycerides (TG) and non-esterified FAs (NEFAs).

(E) Serum cholesterol levels were determined by colorimetric assay.

(F) DNL process was evaluated by measuring FAS and ACC protein expression. Representative blots from indicated time points are shown. Cropped blots are used in the figure. Samples derived from the same experiment and blots were processed in parallel. Results are expressed as mean ± SEM, *p ≤ 0.05, **p ≤ 0.01, ***p ≤ 0.001, ****p ≤ 0.0001; One-Way ANOVA or Kruskall-Wallis test following by a post-hoc test (* compared to SD, # compared to 60% Fruct).

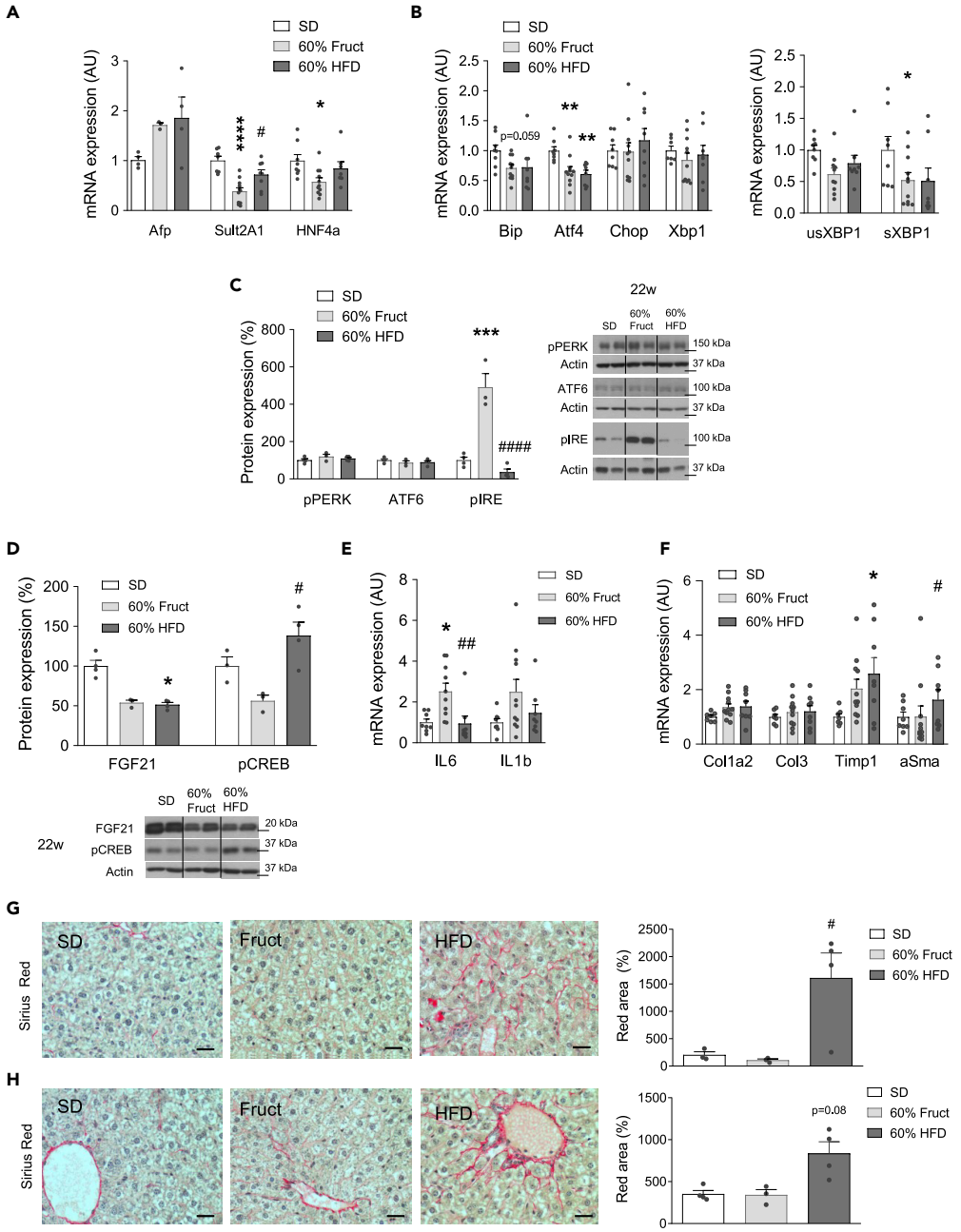

Figure 2. High-fructose diet impairs liver function and triggers inflammation

C57BL/6 female mice fed on SD, 60% Fructose or 60% HFD for 22 weeks (n = 8 per group).

(A) Liver function was evaluated by gene expression of alpha-fetoprotein (Afp), sulfotransferase 2A1 (Sult2A1), and hepatocyte nuclear factor 4 Alpha (Hnf4a).

(B and C) (B) Liver ER stress markers were determined by gene expression of Bip, Atf4, Chop, and total Xbp1(discerning between unspliced usXbp1 and spliced sXbp1) (n = 8 per group), and (C) proteins levels of ATF6 and phosphorylated forms of the ER stress sensor proteins (pPERK and pIRE) (n = 3–4 per group).

(D and E) Liver inflammatory response was analyzed by (D) protein expression of anti-inflammatory related proteins (FGF21 and pCREB) (n = 3–4 per group); and (E) gene expression of pro-inflammatory cytokines IL1b and IL6 (n = 8 per group).

(F) Liver fibrosis was evaluated by gene expression of the fibrotic markers (Col1a2, Col3, Timp1 and aSma) (n = 8 per group).

Figure 2. *Continued*
(G and H) Red positive area was quantified from Red Sirius staining images (Scale bar: 20 μm) to estimate the levels of collagens in livers from different diets in (G) the plate of hepatocytes and (H) nearby liver portal field. Results are expressed as mean ± SEM, *p ≤ 0.05, **p ≤ 0.01, ***p ≤ 0.001, ****p ≤ 0.0001; One-Way ANOVA or Kruskall-Wallis test following by a post-hoc test (* compared to SD, # compared to 60% Fruct).

data suggest that the nature of liver fat depots differ under high-fructose and HFD conditions. Both preclinical models exhibited deterioration of liver function, as shown by increased levels of alpha-fetoprotein (Afp) (Figure 2A), a marker of steatosis and HCC; a potential reduction in bile acid (BA) metabolism, indicated by the significantly reduced levels of sulfotransferase family 2A member 1 (Sult2A1) which mediates the sulfate conjugation of BAs, and hepatocyte nuclear factor 4 alpha (Hnf4a), a master regulator of hepatic function, specifically in animals exposed to high-fructose diet (Figure 2A).

Fructose triggers liver inflammation

As a vital organ for protein synthesis and detoxification, the liver is especially susceptible to ER stress. ER stress takes place when unfolded or misfolded proteins accumulate in the ER lumen. Thus, we analyzed the unfolded protein response (UPR) sensors: Inositol-requiring enzyme 1 (IRE1), protein kinase R-like endoplasmic reticulum kinase (PERK), and activating transcription factor-6 (ATF6), as well as downstream genes, such as binding immunoglobulin protein (Bip), Activating transcription factor-4 (Atf4), CCAAT-enhancer-binding protein homologous protein (Chop) and X-box binding protein (Xbp1) (Figures 2B and 2C). Interestingly, only the IRE sensor was significantly activated by fructose diet (Figure 2C), whereas Bip and Atf4 remained downregulated (Figure 2B). The activation of IRE1 induces splicing of Xbp1 mRNA, which is involved in responding to ER stress. Spliced XBP1 (sXbp1) binds to the endoplasmic reticulum stress elements, which promotes fibroblast growth factor 21 (FGF21) expression. Therefore, ER stress increases FGF21 synthesis as a protective mechanism since this helps to diminish importantly the oxidative stress via activation of ERK and cAMP-responsive element-binding protein (CREB). Our data indicate that this antioxidant mechanism is suppressed by fructose, because Xbp1s, FGF21, and phosphorylated levels of CREB (pCREB) were downregulated (Figures 2B and 2D). It is known that prolonged IRE activation or unresolved ER stress leads to ER stress-induced inflammasome activation and Interleukin 1 beta (IL1b) production, as well as other inflammatory mechanisms mediated by cytokines such as Interleukin 6 (IL6). Thus, we examined IL-6 and IL1b expression and found a significant increase in fructose-fed animals (Figure 2E). These results indicate that high levels of pIRE in fructose diet are accompanied by activation of inflammation-induced pathogenic ER stress pathways (Figure 5A). Moreover, we also analyzed markers of liver fibrosis such as collagen type 1 alpha 2 (Col1a2), collagen type III (Col3), tissue inhibitor of metalloproteinase-1 (Timp1), and alpha-smooth muscle actin (aSma) in our experimental model (Figure 2F). The results obtained suggested that, unlike HFD, fructose diet had an insignificant effect on the progression of liver fibrosis (Figures 2F–2H).

Specific liver GLUT8 silencing reduces fructose-induced NAFLD

It has been previously described that global GLUT8KO female mice exhibit attenuated fructose-induced hepatic TG and cholesterol accumulation (Debosch et al., 2014). To test whether this was an intrinsic liver effect, we assessed if targeted depletion of liver GLUT8 was sufficient to prevent the fructose-induced steatosis phenotype in C57BL/6 females. First, we validated the zone-specific GLUT8 knockdown after administration of Cont-Fruct or shG8-Fruct lentiviruses, using a specific antibody against GLUT8 (Figure S5 and Table S3). Immunohistochemistry analysis revealed a 79% reduction of liver immuno-positive signal in the shG8 animals (Figure 3A) and this reduction in Glut8 expression was specifically within the liver (Figures S6A and S6B). After this Glut8 silencing, there was an increased expression of both Glut2 and Glut5 (Figure S7). This upregulation in fructose transporters could be explained as a regulatory mechanism to compensate for the silencing of Glut8 and/or may be an insight that the GLUT8-knockdown recapitulates a more normo-physiological liver condition, gaining prominence the two well-established glucose and fructose transporters.

Under fructose diet, the hepatic GLUT8 knockdown reduced lipid content, as shown by the lack of white lipid droplets in liver slides stained with H&E (Figure 3B), lower liver weight (Figure 3B), decreased liver TG (Figure 3D) and significant reduction of Oil Red staining (Figure 3E); and further supported by serum TG (Figure 3F) and reduced cholesterol levels (Figure 3G). These results demonstrated a dramatic reduction in FA stores. Unexpectedly, we also observed a decreased in genes involved in fibrosis (Figure 3H), supported by Sirius staining (Figure 3I).

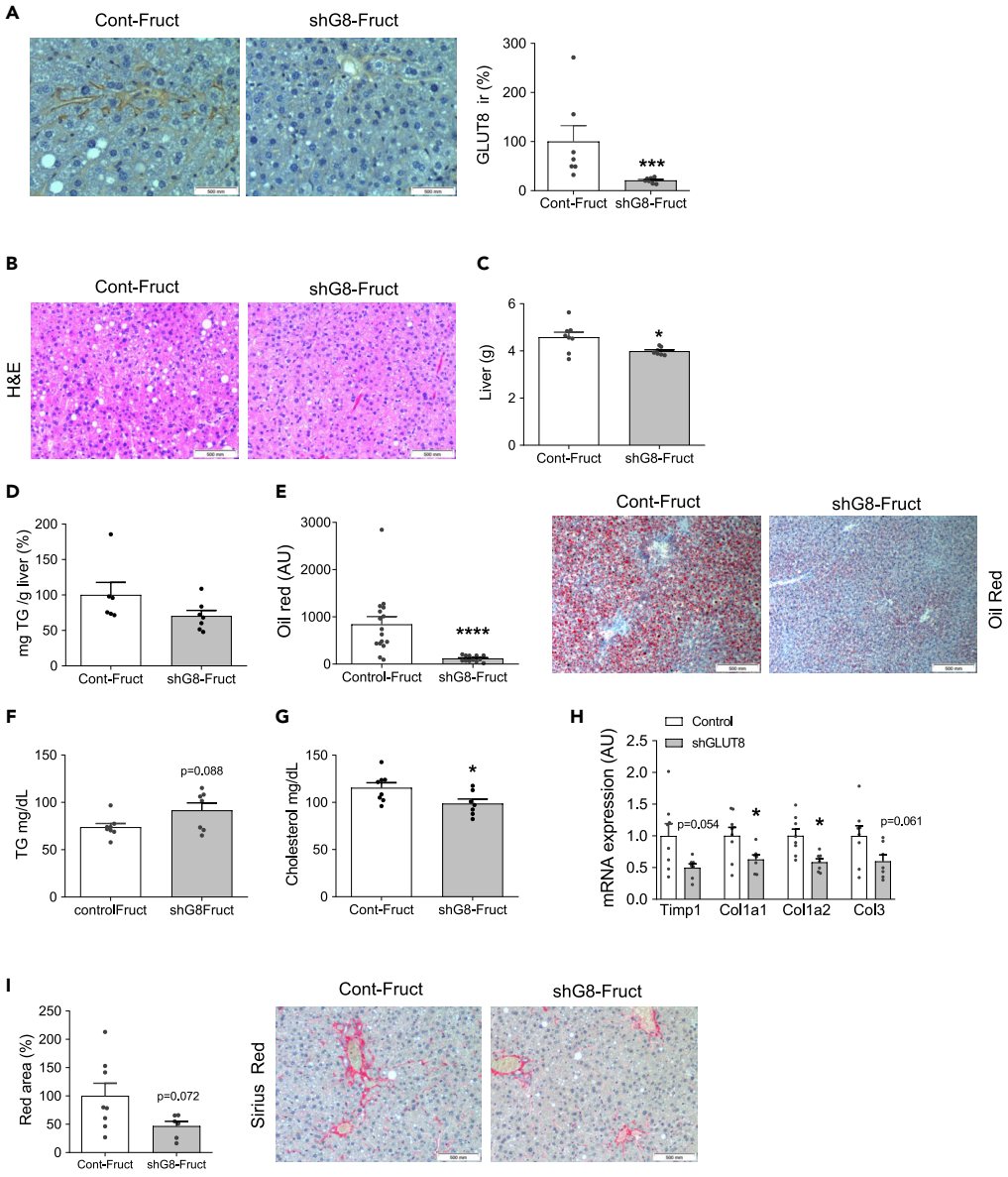

Figure 3. Liver GLUT8 silencing reduces steatosis and fibrosis

C57BL/6 female mice received a tail vein injection of 1x106 TU/mL lentiviral particles to inhibit Slc2A8 (shG8-Fruct) or to use as control (Cont-Fruct), and fed with 60% Fructose diet for 22 weeks (n = 7–8 per group).

(A–E) (A) Specific silencing of liver GLUT8 was tested by immunohistochemistry GLUT8 protein expression (scale bar: 20 μm). Liver FA accumulation was evaluated by (B) H&E staining (scale bar: 50 μm), (C) liver weight (G), (D) TG content in liver and (E) Oil Red staining (scale bar: 100 μm).

(F and G) Circulating levels of (F) TG and (G) cholesterol (mg/dL).

(H and I) Liver fibrosis was evaluated in terms of (H) genetic expression of key biomarkers (Timp1, Col1a1, Col1a2, and Col3) and (I) Sirius red staining taking the portal vein into account. *p ≤ 0.05, **p ≤ 0.01, ***p ≤ 0.001P, ****p ≤ 0.0001; unpaired t test or Mann-Whitney test.

Omega oxidation is upregulated by the inhibition of liver GLUT8

To establish a metabolic signature and to understand the mechanisms underlying the role of GLUT8 in NAFLD development, we performed a quantitative proteomic analysis using SWATH technology. Moreover, this analysis took account of an enriched-membrane and cytosolic protein fractions. Venn diagrams represent common and unique proteins in Cont-Fruct and shG8-Fruct livers (Figure 4A). We focused our

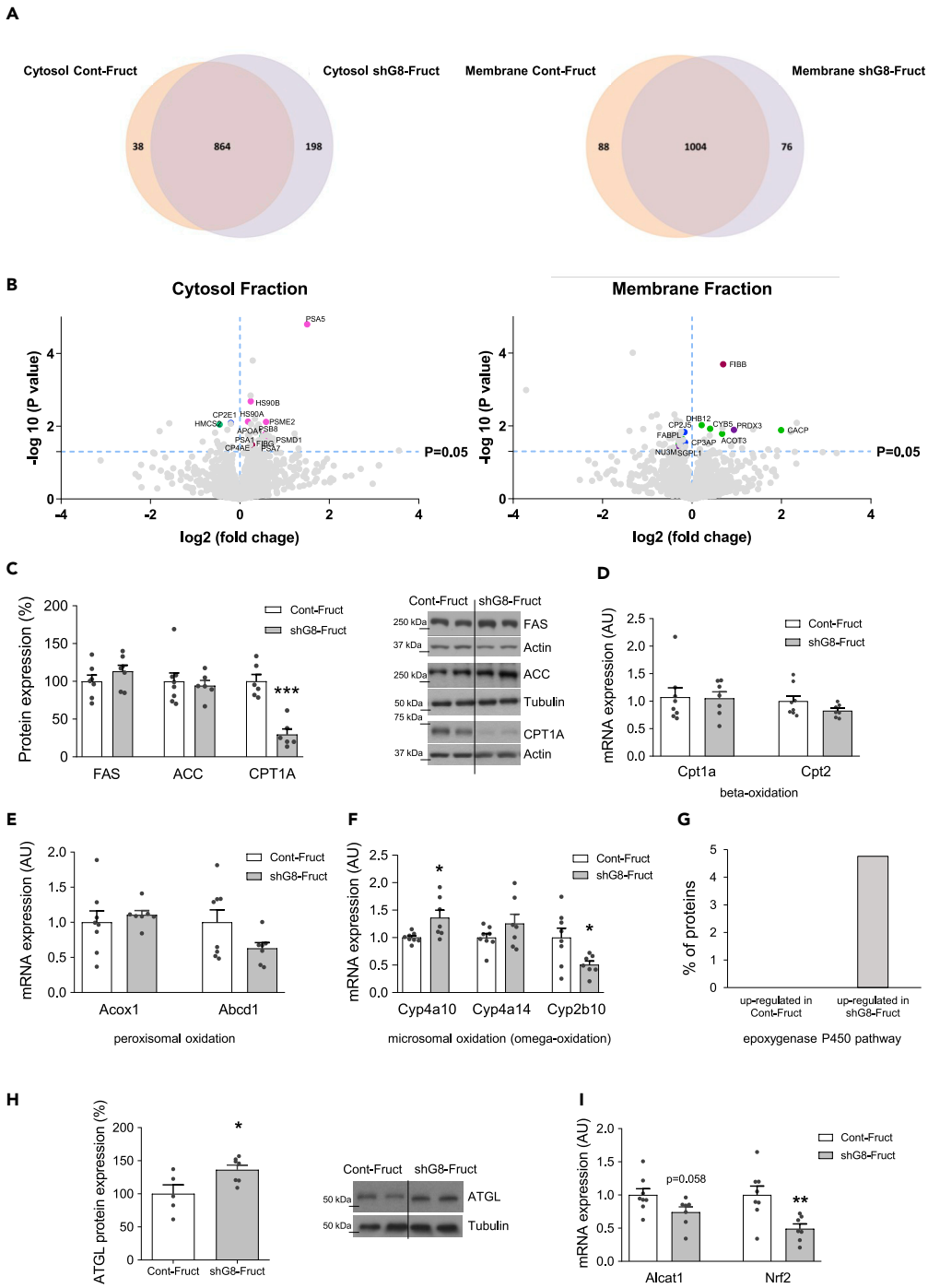

Figure 4. Under the high-fructose diet, liver GLUT8 knockdown promotes the omega oxidation and lipolysis

C57BL/6 female mice received a tail vein injection of 1x106 TU/mL lentiviral particles to inhibit Slc2A8 (shG8-Fruct) or to use as control (Cont-Fruct), and fed with 60% Fructose diet for 22 weeks (n = 7–8 per group).

(A) The Venn diagram illustrates common and unique proteins in control (Cont-Fruct) and liver GLUT8 knockdown (shG8-Fruct) in both cytosol and membrane enriched fractions.

(B) Volcano plot of quantitative proteomic data from cytosol and membrane fractions. Volcano plots are depicted with the fold change and p value calculated by t test. The averages of Cont-Fruct group (n = 4) were compared with the average of the data from shG8 group (n = 4).

Figure 4. *Continued*

(C–F) (C) Lipid metabolism was evaluated by protein expression of FAS, ACC, and CPT1A, and by (D) gene expression of beta-oxidation (Cpt1a, Cpt2) markers. Gene expression of essential components of (E) peroxisomal and (F) omega oxidation.

(G) Regulation of the epoxygenase P450 pathway in shG8-Fruct group compared to Cont-Fruct.

(H) The liver lipolysis was evaluated by ATGL protein expression.

(I) The oxidative stress was assayed by the gene expression of Alcat1 and Nrf2. Results are expressed as mean ± SEM. *p ≤ 0.05, **p ≤ 0.01, ***p ≤ 0.001; unpaired t test or Mann-Whitney test. Black line represents cropped blots.

analysis on proteins upregulated in the following processes: (1) lipid metabolism, (2) endoplasmic reticulum-associated protein degradation (ERAD), (3) cytochrome P450 superfamily, (4) oxidative stress, and (5) fibrosis (Table 1, and Figure 4B).

Significantly upregulated proteins in Cont-Fruct mice (fold-change > 1) included: carnitine O-acetyltransferase and acyl-coenzyme A thioesterase 3, which regulates intracellular levels of acyl-CoA; cytochrome b5, which in turn contributes to the sterol biosynthetic pathway; and very-long-chain 3-oxoacyl-CoA reductase, which participates in the production of VLCFAs. These findings, alongside supplementary data concerning biological processes involved in lipid metabolism (Figure S8), support the idea that *de novo* lipogenesis (DNL) was upregulated in Cont-Fruct mice compared to shG8-Fruct mice. Proteasome subunits also prevailed in the Cont-Fruct group (Table1), suggesting an enhanced activation of the ERAD system. Fibrinogen gamma and beta were also upregulated in this group (Table1), in agreement with Sirius staining (Figure 3I). In contrast, significantly upregulated proteins in shG8-Fruct mice (fold-change < 1) comprised cytochromes P450 monooxygenases involved in the metabolism of FAs, including cytochrome P450 2E1 and 4A14, which hydroxylate FAs specifically at the omega-1-position and display the highest catalytic activity for saturated FAs; or cytochrome P450 3A25 that oxidizes a variety of unrelated compounds, such as steroids and FAs; and cytochrome P450 2J5 with oxidoreductase activity (Table 1, and Figure 4B). While the main mechanism linked to beta-oxidation such as CPT1A was downregulated (Figures 4C and 4D), other members of the cytochrome P450 superfamily, such as Cyp4a10 and Cyp4a14, were also enhanced according to gene expression analysis (Figure 4F). In concordance, a comparative study using a FunRich program denoted that proteins involved in the epoxygenase P450 pathway were highly upregulated in shG8-Fruct mice (Figure 4G). Interestingly, when we checked genes involved in the mitochondrial beta-oxidation, such as Cpt1a and carnitine palmitoyltransferase 2 (Cpt2), or peroxisomal oxidation of VLCFAs mediated by Acyl-coenzyme A oxidase-1(Acox1) and ATP binding cassette subfamily D member 1 (Abcd1), we did not observe any significant differences after liver GLUT8 knockdown (Figures 4D and 4E). We also analyzed lipolysis and observed that ATGL protein levels were significantly increased under the inhibition of liver GLUT8 (Figure 4H). These results indicate major lipid oxidation and mobilization in the absence of liver GLUT8, where omega oxidation seems to plays an important role. In addition, when GLUT8 was silenced in the liver, we observed a general attenuation of glucose metabolism, although there was still gluconeogenesis activation in the membrane fraction (Figure S9).

Hepatic GLUT8 knockdown reduces oxidative stress and decreases the inflammation/inflammasome linked to pIRE over activation

Analysis of the oxidative stress process using SWATH analysis revealed that the NADH-ubiquinone oxidoreductase chain 3 protein (NAD3), which mediates the transfer of electrons from NADH to the respiratory chain was upregulated in shG8-Fruct animals, whereas, in Cont-Fruct mice upregulation of the mitochondrial thioredoxin-dependent peroxide reductase (PRDX3), which is involved in cell protection against oxidative stress (Figures 4B and Table 1), confirmed the presence of fructose-induced oxidative stress and mitochondrial dysfunction in a Glut8-dependent manner. Further evidence of fructose-induced oxidative stress is shown in the biological processes affected (Figure S10A) and gene expression of oxidative stress markers such as lysocardiolipin acyltransferase 1 (Alcat1) and nuclear factor erythroid 2-related factor 2 (Nrf2) in the livers of Cont-Fruct *vs* shG8-Fruct mice. Alcat1(usually upregulated in mouse models of NAFLD) and Nrf2 (that orchestrates an antioxidant response) were downregulated in shG8-Fruct mice (Figure 4I).

Both, oxidative stress and ER stress contribute to the process of liver inflammation. In fact, the data obtained indicate that fructose pIRE-induced pathological ER stress switches to an adaptative/recovery ER stress-mediated by ATF6 (Figure 5A). Interestingly, the examination of the ER stress markers after liver GLUT8 silencing show that, unlike pIRE and CHOP, proteins such as ATF6 and BIP were markedly

Table 1. Proteins upregulated in control-fructose (fold change >1) and upregulated in shG8-Fructose (fold-change < 1) in the cytosol and membrane isolated fractions

Class		Protein symbol	Uniprot ID	Protein name	Fold change	p value
Cytosol	Lipid metabolism	APOA1	Q00623	Apolipoprotein A-I	1.41	1.95E-02
		HMCS2	P54869	Hydroxymethylglutaryl-CoA synthase	0.73	8.93E-03
	ERAD	PSA5	Q9Z2U1	Proteasome subunit alpha type-5	2.83	1.58E-05
		PSMD1	Q3TXS7	26S proteasome non-ATPase regulatory subunit 1	1.56	2.24E-02
		PSME2	P97372	Proteasome activator complex subunit 2	1.49	7.61E-03
		PSB8	P28063	Proteasome subunit beta type-8	1.47	1.67E-02
		PSA7	Q9Z2U0	Proteasome subunit alpha type-7	1.34	4.73E-02
		PSA1	Q9R1P4	Proteasome subunit alpha type-1	1.24	4.41E-02
		HS90B	P11499	Heat shock protein HSP 90-beta	1.18	2.06E-03
		HS90A	P07901	Heat shock protein HSP 90-alpha	1.13	7.46E-03
		BAP31	Q61335	B-cell receptor-associated protein 31	0.00	4.26E-02
	Cytochrome P450	CP2E1	Q05421	Cytochrome P450 2E1	0.86	8.14E-03
		CP4AE	O35728	Cytochrome P450 4A14	0.74	3.55E-02
	Fibosis	FIBG	Q8VCM7	Fibrinogen gamma chain	1.20	3.27E-02
Membrane	Lipid metabolism	CACP	P47934	Carnitine O-acetyltransferase	3.98	1.30E-02
		ACOT3	Q9QYR7	Acyl-coenzyme A thioesterase 3	1.59	1.63E-02
		CYB5	P56395	Cytochrome b5	1.32	1.19E-02
		DHB12	O70503	Very-long-chain 3-oxoacyl-CoA reductase	1.16	9.45E-03
		FABPL	P12710	Fatty acid-binding protein, liver	0.85	2.25E-02
		SGPL1	Q8R0X7	Sphingosine-1-phosphate lyase	0.40	4.93E-02
		AAKG1	O54950	5'-AMP-activated protein kinase subunit gamma-1	0.00	4.64E-02
	Cytochrome P450	CP3AP	O09158	Cytochrome P450 3A25	0.89	2.84E-02
		CP2J5	O54749	Cytochrome P450 2J5	0.88	1.47E-02
	Oxidative stress	PRDX3	P20108	Thioredoxin-dependent peroxide reductase	1.91	1.28E-02
		NU3M	P03899	NADH-ubiquinone oxidoreductase chain 3	0.80	3.81E-02
	Fibosis	FIBB	Q8K0E8	Fibrinogen beta chain	1.62	2.03E-04

upregulated (Figures 5B and 5C). These results were supported by FunRich comparative analysis indicating the contribution of the main biological processes in Cont-Fruct and shG8-Fruct involved in ER stress (Figure S10B).

Next, we evaluated the liver inflammatory response by mRNA expression of IL6, EGF-like module-containing mucin-like hormone receptor-like-1 (F4/80), Interleukin 15 receptor, tumor necrosis factor-alpha, and tumor growth factor-beta. We observed that fructose-induced inflammation was significantly reduced under the lack of GLUT8 (Figure 5D). Similarly, ablation of liver GLUT8 reduced the expression of inflammasome markers such as IL1b, NOD-, LRR- and pyrin domain-containing protein 3 (Nlrp3), the adapter protein Asc (apoptosis-associated speck-like protein containing a CARD), and Interleukin 18 (IL18) (Figure 5E). In addition, protein levels of cleaved Caspase1, an enzyme that proteolytically cleaves precursors of the inflammatory cytokines IL1b and IL18 were significantly reduced (Figure 5F). Accordingly, we also observed that pCREB, which has anti-inflammatory functions (Wen et al., 2010), was enhanced (Figure 5G).

The inhibition of GLUT8 affects human LX2 and THLE2 cells differently

There are four major liver cell types which spatiotemporally cooperate to shape and maintain liver functions (HCs, hepatic stellate cells (HSCs), Kupffer cells, and liver sinusoidal endothelial cells. Since HCs comprise 55-65% of the liver's mass, and HSCs have a remarkable range of functions in normal and injured liver, so we explored the cell type-specific roles of GLUT8 in the liver by examining GLUT8 expression and its impact on

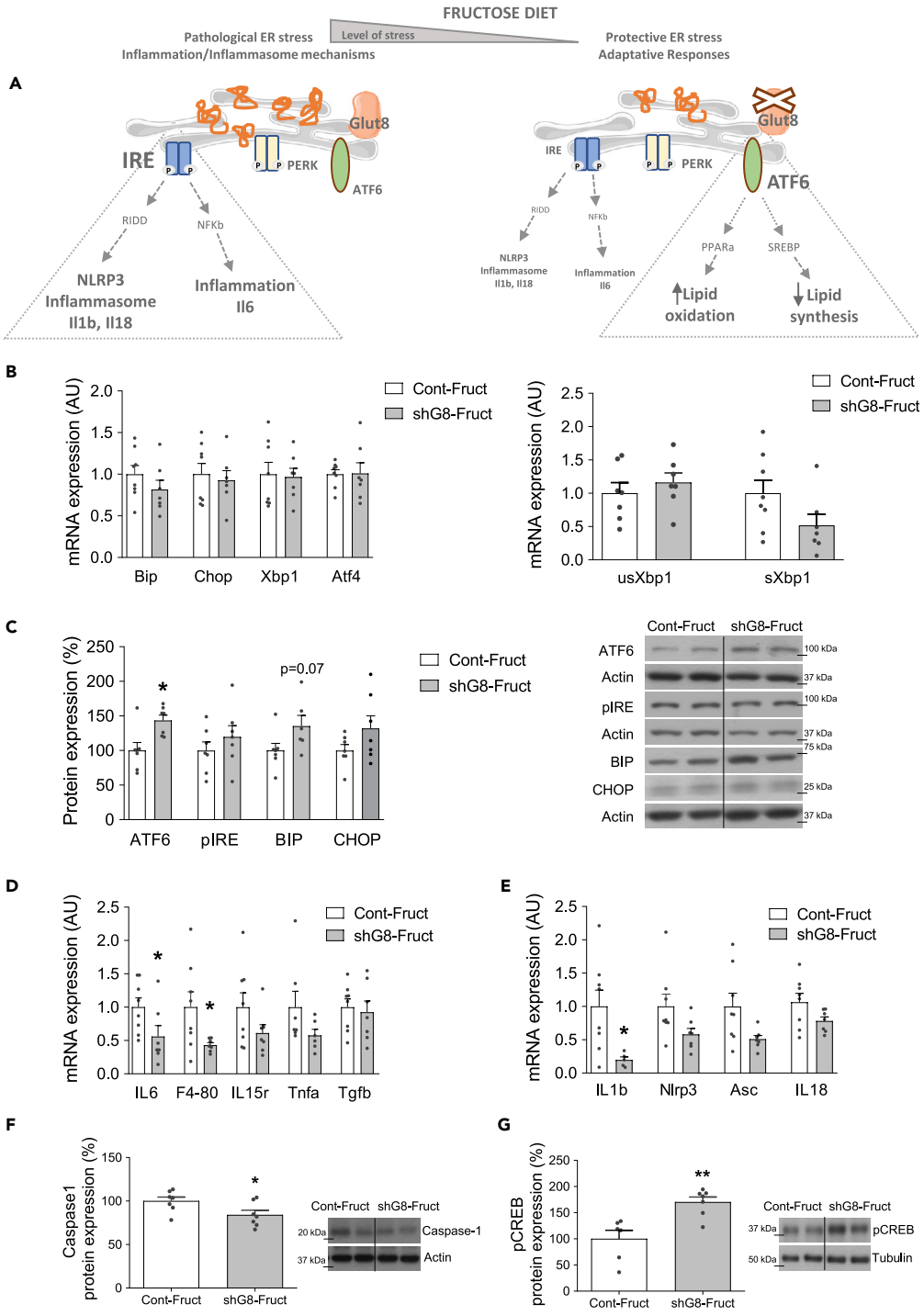

Figure 5. Liver GLUT8 knockdown improves ER stress and decrease inflammation/inflammasome induced by fructose diet

C57BL/6 female mice received a tail vein injection of 1x106 TU/mL lentiviral particles to inhibit Slc2A8 (shG8-Fruct) or to use as control (Cont-Fruct) and fed with 60% Fructose diet for 22 weeks (n = 7–8 per group).

(A) Schematic representation of the switched ER stress mechanism observed after GLUT8 knockdown.

(B and C) (B) Expression of the main genes involved in ER stress signaling including usXbp1 and uXbp1, and (C) protein levels of ATF6 and phospho-IRE ER stress sensors, chaperones (GPR78/BiP), and the C/EBP Homologous Protein (CHOP) Transcription Factor.

Figure 5. *Continued*

(D and E) Inflammation measured by gene expression of (D) IL6 and IL15 receptor produced during the immune response, a major macrophage marker (F4-80), tumor necrosis factor-alpha (Tnfa), and transforming growth factor-beta (Tgfb); and (E) gene expression of inflammasome markers (IL1b, Nlrp3, Asc, IL18).

(F) protein expression of Interleukin-1 converting enzyme (Caspase 1), that proteolytically cleaves precursors of the inflammatory cytokines IL1b and IL18.

(G) Protein levels of the phosphorylated form of cAMP response element-binding protein (CREB). Results are expressed as mean ± SEM. *p ≤ 0.05, **p ≤ 0.01, ***p ≤ 0.001P; unpaired t test or Mann-Whitney test.

cellular function impact on HCs and HSCs using established hepatic cells lines cultures (AML12 mouse HCs, human LX2 HSCs, and human THLE2 HCs). Immunohistochemistry confirmed the presence of GLUT8 in AML12 and LX2 cells (Figure 6A), so then we analyzed GLUT8 mRNA and protein expression in LX2 and AML12 cells under different media mimicking the SD (physiologycal glucose concentration), fructose-enriched or HFD-like conditions (Figure 6B). Fructose-enriched medium upregulated GLUT8 expression in LX2 cells, whereas in AML12 cells GLUT8 was downregulated (Figures 6C and 6D). The inflammation markers induced by fructose in the *in vivo* studies are also significantly upregulated in LX2 cells (Figure 6E). Moreover, the expression of the genes of the intercellular adhesion molecule 1 (ICAM1) and the disintegrin and metalloproteinase 17 (ADAM17) involved in inflammation and well-known markers of HSCs activation was also elevated (Figure 6F). LX2 cells showed an unexpected intracellular GLUT8 localization pattern, so an as-yet-unknown intracellular role of GLUT8 in hepatic cells cannot be ruled out. Indeed, parallel studies point to the presence of GLUT8 in the late endosomal/lysosomal compartments (Figure S11) as has been demonstrated in other tissues, such as the testis (Diril et al., 2009). Next, we used human siRNA to silence GLUT8 in LX2 and human HCs THLE2 cells and looked at gene expression of DNL, lipolysis, oxidation, and inflammation markers after 24hr fructose exposure (Figure 7A). The efficiency of GLUT8 silencing was around 50% in LX2 (Figures 7B) and 75% in THLE2 (Figure 7E) cells. GLUT8 knockdown in LX2 cells significantly decreased IL6 gene expression (Figure 7B), indicating a reduction of inflammatory signals (Figure 7C). Interestingly, whilst the human cytochrome P450 monooxygenase CYP4F2, which predominantly catalyzes the omega-oxidation of long Fas and VLCFAs, was significantly reduced in GLUT8 silenced LX2 cells; CYPA11 and CYP4F3, which are involved in the metabolism of various endogenous substrates, including FAs and their oxygenated derivatives (oxylipins), were upregulated (Figure 7D). In THLE2 cells, GLUT8 knockdown cells significantly decreased IL1b and IL18 gene expression (Figure 7F), indicating that the activation of the inflammasome response was reduced. Importantly, the gene expression of the three cytochrome P450 monooxygenases analyzed was downregulated (Figure 7G). GLUT8 silencing mainly reduced fructose-induced DNL in THLE2 cells, since the fatty acid synthase (FASN) gene expression and FAS and ACC protein levels were downregulated (Figures 7H and 7I). Enhanced beta-oxidation mediated by CPT1A and lipolysis by ATGL was only observed in LX2 cells (Figure 7J). Altogether, these results indicate that the inhibition of GLUT8 differently reduces the FA content in both LX2 and THLE2, as confirmed by Oil Red staining (Figure 7K), probably due to reduced lipogenesis in HCs and enhanced lipid oxidation and lipolysis in stellate cells.

DISCUSSION

Within the heterogeneity in NAFLD risk profiles, the diet consumed and differences in how it is metabolized constitute a key factor for the accurate identification of high-risk individuals and personalized preventive/therapeutic strategies. Female subjects seem to be more sensitive to fructose metabolism, hence one of these strategies may be the reduction of liver fructose intake achieved by sugar facilitated transporters (GLUT family) across the cell membranes. Fructose metabolism involves its conversion into glucose and studies have showed that elevated fructose consumption is more cytotoxic than glucose (Ter Horst and Serlie, 2017). This conversion is only partly carried out in intestinal cells, thus, at higher luminal concentrations, fructose is metabolized in the liver. There, fructolysis bypasses the step using glucokinase and is much faster than glycolysis, thus providing increased substrate for all central carbon metabolic pathways, including glycolysis, glycogenesis, gluconeogenesis, lipogenesis, pentose phosphate pathway, and oxidative phosphorylation (Hannou et al., 2018). On the other hand, fructose rather than glucose induces barrier deterioration of the intestinal epithelial cells (IECs). Moreover, fructose metabolites trigger ER stress and inflammation in both in IECs and in HCs. Noteworthy ER-stress-activated IRE1 and TNF signaling stimulate hepatosteatosis (Todoric et al., 2020).

Besides glucose transporter 2 (GLUT2) and glucose transporter 5 (GLUT5), a previous study based on a germ-line GLUT8 knock-out mouse model recognized GLUT8 as a liver fructose transporter that mediates

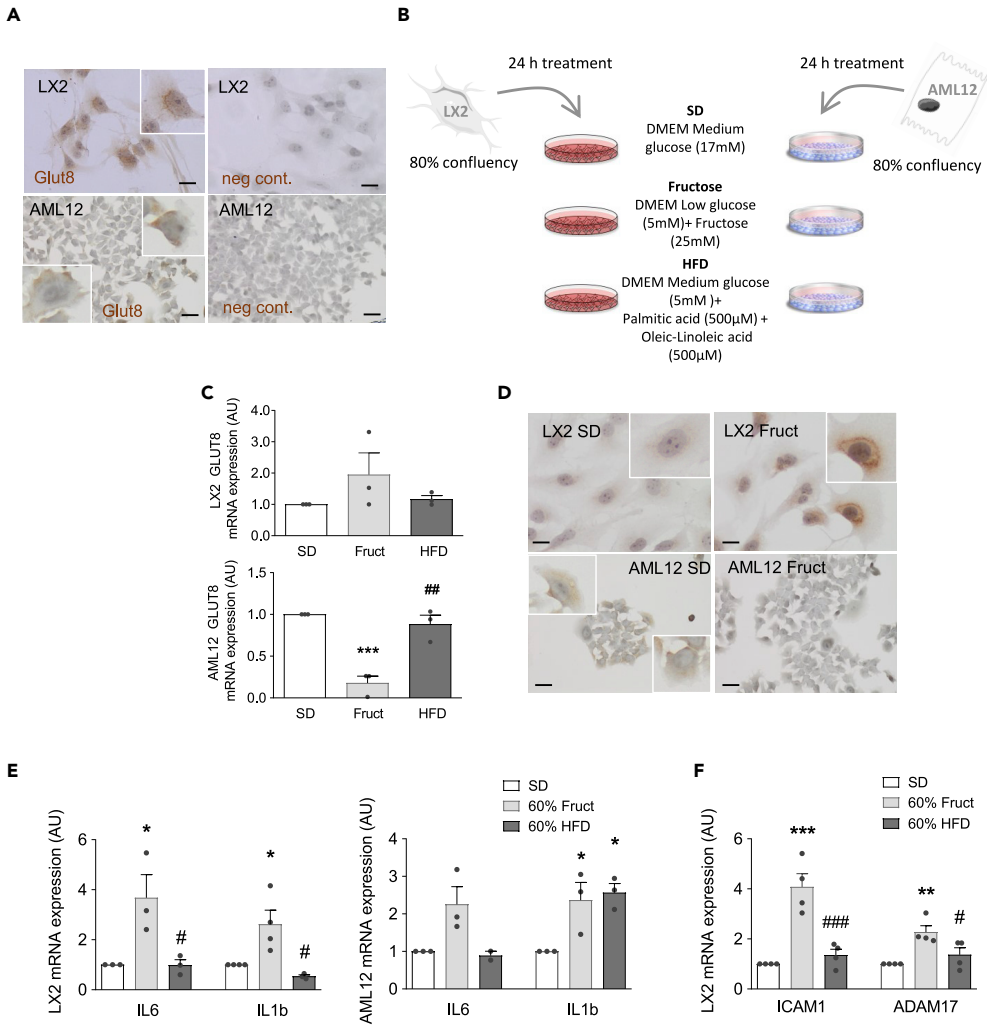

Figure 6. GLUT8 is differentially regulated by fructose in LX2 and AML12 cells

Fructose induces inflammation in both cell types.

(A) GLUT8 expression assayed by immunohistochemistry in human stellate cells (LX2) and mouse hepatocytes (AML12) (n = 3) and their negative controls (neg cont.) in basal media (scale bar: 20 µm).

(B) Schematic depiction of 24hr cells treatments with different nutrients.

(C and D) Regulation of Glut8 mRNA under basal (SD), Fructose (Fruct.), and high-fat (HFD) media; (C) quantification of mRNA and (D) representative images of immunohistochemistry.

(E) Genetic expression in hepatic stellate cells (LX2) and hepatocytes (AML12) of the main cytokines involved in the inflammatory response (IL6) and inflammasome (IL1b) activation.

(F) Genetic expression in LX2 of other inflammatory markers, ICAM1 and ADAM7. Results are expressed as mean ± SEM, *p ≤ 0.05, **p ≤ 0.01, ***p ≤ 0.001; One-Way ANOVA or Kruskall-Wallis test following by a post-hoc test (* compared to SD, # compared to 60% Fructose).

fructose-induced DNL and macrosteatosis in female mice (Debosch et al., 2014). In our study, we achieved a liver-targeted GLUT8 silencing in order to understand better the role of this new player in NAFLD progression. Our results, in a fructose-induced female NASH model, demonstrated a surprising recovery of the inflammatory/ER stress status in liver GLUT8-knockdown animals. We observed a reduced liver weight, decreased hepatic FA, plasma cholesterol levels, and, curiously, improvement of the fibrotic state. These effects could be explained by (1) the reduction of DNL, (2) the increased FA oxidation, or (3) maybe both. In our experimental model, we have not observed significant changes in FAS and ACC expression despite the reduction in liver steatosis. Nevertheless, after GLUT8 silencing, the inflammation process decreased

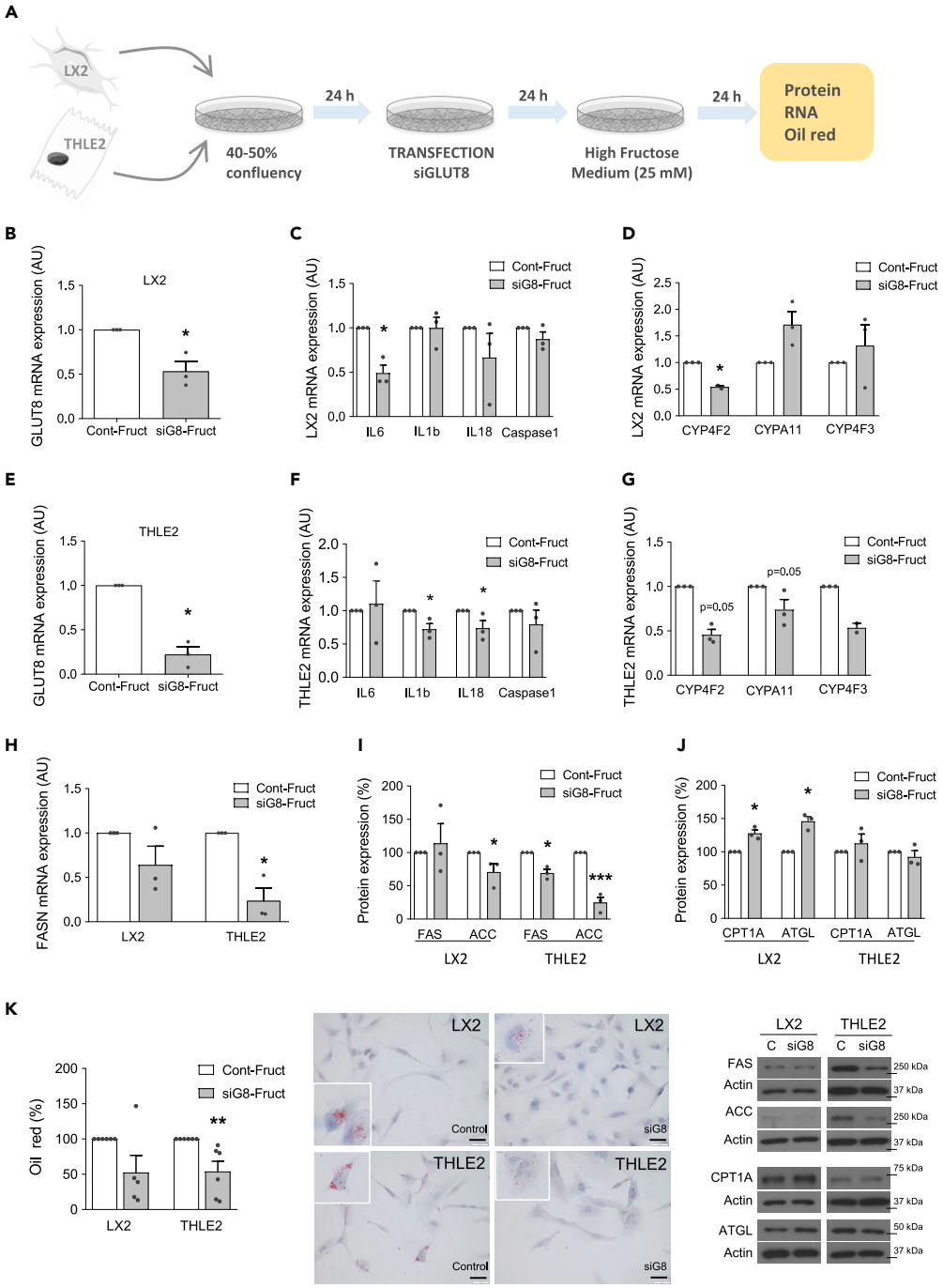

Figure 7. GLUT8 silencing in hepatic human cells in fructose media reduces DNL in THLE2 hepatocytes, increases oxidation/lipolysis in LX2 stellated cells and ameliorates inflammation in both

(A) Schematic representation of the experimental process.

(B–-D) Impact of GLUT8 silencing in LX2 cells and its effects on (C) mRNA expression of inflammatory-related genes, and (D) human cytochrome P450-related omega-oxidation, after 24hr incubation in fructose media (n = 3 independent experiments conducted by triplicate).

(E–G) Impact of GLUT8 silencing in THLE2 cells and its effects on (F) inflammation markers, and (G) expression of cytochrome P450 monooxygenases involved in the metabolism of FAs after 24hr fructose enriched media (n = 3 independent experiments conducted by triplicate).

Figure 7. *Continued*

(H–J) Lipid metabolism in LX2 and THLE2 cells after GLUT8 knockdown assayed by (H) gene expression of FASN and protein expression of (I) lipogenic (FAS, ACC) and (J) lipolytic (CPT1A, ATGL) factors. Representative blots are shown (bellow J).

(K) Measure of lipid content in LX2 and THLE2 cells by Oil Red staining (scale bar: 20 μm). Results are expressed as mean ± SEM. *p ≤ 0.05, **p ≤ 0.01, ***p ≤ 0.001P; unpaired t test or Mann-Whitney test.

markedly. In agreement with recent data, this decrease could explain the reduction in liver steatosis present in GLUT8-knockdown mice (Todoric et al., 2020). Additionally, an upregulation of the cytochrome P450 epoxygenase pathway and increased ATGL activity indicate major oxidation and lipolysis of accumulated FAs.

It is known that malonyl-CoA generated via DNL limits FA oxidation by inhibiting CPT1A, the enzyme required for translocation of long-chain fatty acids into the mitochondria (Hannou et al., 2018). However, when beta-oxidation is impaired due to fructose-induced defects in CPT1A mechanisms, the silencing of liver GLUT8 promotes a subsidiary pathway for maximal fat oxidation: omega oxidation (Miura, 2013). This unusual FA oxidation is carried out by the liver, kidney and lung, as demonstrated in microsomal preparations from mice and other species (Ichiha et al., 1969). The proposed biological significance of omega-oxidation is the generation of more soluble acids that are easily secreted into the blood and finally excreted in the urine (Miura, 2013). Mortensen et al. (Mortensen, 1980) demonstrated that omega oxidation of FAs might have important metabolic influence in situations where living organisms lacked carbohydrates and largely have to utilize fats for energy demand. Despite the idea that omega oxidation catalyzed by Cyp2E1, Cyp 4A10, and Cyp 4A14 constitutes a mechanism of lipid-induced cellular injury in NAFLD due to formation of ROS species (Browning and Horton, 2004), many other studies consider FA omega oxidation a rescue pathway for FA oxidation disorders in humans (Wanders et al., 2011). Moreover, the cytochrome P450 epoxygenase pathway regulates hepatic inflammatory response in fatty liver disease (Schuck et al., 2014). At least, in our female fructose model, the upregulation of the murine cytochrome P450 epoxygenase pathway seems to have a protective effect against liver steatosis.

Importantly, steps in DNL and very-low-density lipoprotein synthesis occur at the ER membrane; thus, fructose-induced lipogenesis may elicit an ER stress response that contributes to NAFLD pathogenesis and progression (Malhi and Kaufman, 2011). As a vital organ for protein synthesis and detoxification, the liver is especially susceptible to ER stress. The signaling initiated by IRE and other UPR pathways can restore homeostasis, however, prolonged or unresolved ER stress leads to inflammation via the sustained interaction of IRE and TNF receptor-associated factor 2 (TRAF2), leading to NFkB activation (Guo and Li, 2014). As a consequence, IRE is a key partner in the ER stress-induced inflammasome and inflammasome-independent inflammation mechanisms. Indeed, in our study, the exacerbated fructose-induced activation of IRE was accompanied by increased IL1b and IL6 gene expression. Unexpectedly, after inhibition of GLUT8 in the liver we observed ATF6 activation and enhanced BIP protein levels. Although ER stress pathways are usually associated with their pathogenic effects, this result is not unusual taking the protective role of UPR activation to maintain homeostasis into account (Cinaroglu et al., 2011). In fact, in murine models, it has been shown that the activation of the ATF6 pathway protects against hepatic steatosis, via activation of PPAR-alpha stimulating FA oxidation under high-fat, high-sucrose diet (Chen et al., 2016). Moreover, glucose deprivation activates ATF6 but suppresses the SREBP-2 regulated transcription and, consequently, its lipogenic effect (Zeng et al., 2004).

One of the unresolved issues from our *in vivo* study relates to the liver cell types involved in the fructose-induced liver injury and its prevention by silencing GLUT8. GLUT8 is expressed in both, HCs and HSCs, and their intracellular localization is not surprising since it coincides with previous findings in other cell types (Schmidt et al., 2009). Our *in vitro* studies support that the absence of GLUT8 impacts lipid metabolism in human HCs and stellate cells differentially: reducing lipogenesis in THLE2 cells while promoting FA oxidation in LX2 cells, respectively. This dual effect may explain the potent diminution of fat content observed in the liver.

In summary and based on our data we hypothesize that the lack of GLUT8 in liver mimics a cellular glucose/fructose deprivation state, which in turn modulates lipogenesis and promotes FA oxidation as a source of

energy. Limited carbohydrates availability in liver cells may be achieved by 1) reduced fructose uptake in the plasma membrane of HCs as previously described, but importantly also by (2) the impaired intracellular import/export via facilitative transporters such as GLUT8. Since beta-oxidation mediated by CPT1A mechanisms is compromised under the fructose diet, and alternative pathways, omega-oxidation and lipolysis, are used to breaking fat. Beyond lipid metabolism, fructose-induced pathogenic ER stress, and inflammation/inflammasome are attenuated in the absence of GLUT8, preventing the first steps of NAFLD development. Whilst HCs are mainly involved in relation to lipogenesis, stellate cells GLUT8 appears mainly to regulate lipid oxidation; however, our data indicate that both cell types are involved in terms of the inflammatory response. Interestingly, while rich fructose medium induces a high HSCs activation that over time results in the formation of liver fibrosis (Koyama and Brenner, 2017), GLUT8 silencing reduces ACC expression in LX2 cells that could suppress the activation of these cells and thus the fibrosis process (Bates et al., 2020).

This study may serve as a warning against excessive consumption of sugar-sweetened beverages and manufactured food products containing high-fructose corn syrup; as this may lead to potential pathophysiological consequences, especially in females due to greater susceptibility to fructose uptake and metabolism by the liver. In addition, this study provides a drug target with the potential to prevent fructose-induced liver injury and raises the question whether, given the high energy demand for the proliferation of liver tumor cells, restriction of carbohydrate supply mediated by GLUT8 and, in turn, diminution of fat sources, may slow down HCC progression.

Limitations of the study

Our study contributes to a better understanding of the role of GLUT8 in the development of NAFLD in the context of high amounts of fructose diet intake. Despite liver-specific knockdown of GLUT8 improves liver fat deposition, lipotoxicity, and inflammation in female mice, we have not provided potential mechanisms to explain why female mice seem to be more responsive to high fructose diet than male mice. Future studies should also include a model in male mice to address possible discrepancies between fructose consumption and sex-specific effects. Moreover, the logical approach will be to compare male and females with/without gonadectomy and with/without replacement therapy in order to uncover the molecular underpinning of these sex differences. Similarly, a high fructose diet is only one of the diet-induced NAFLD animal models and does not recapitulate all NAFLD human features. It would be interesting to elucidate in further studies using an American lifestyle-induced obesity syndrome or cafeteria diets, which are more representative of human habits, whether the beneficial effects of hepatic GLUT8 silencing can be replicated. Of note, consideration of the deleterious effects of fructose intake, including the gender-related one, also needs to be refined taking into account that the end-alterations in liver function are multifactorial and the impact of fructose may be related to other factors, such as age, previous or concurrent diet, timing, dosage, and also dependent of other co-morbidities. In order to extrapolate the conclusions of this study, all these limitations should be considered.

Resource availability

Lead contact

Further information and requests for resources and reagents should be directed to and will be fulfilled by the lead contact Amparo Romero-Picó (amparo.romero@usc.es).

Materials availability

This study did not generate new unique reagents.

Data and code availability

All data supporting the current study are available from the corresponding author on request.

METHODS

All methods can be found in the accompanying Transparent methods supplemental file.

SUPPLEMENTAL INFORMATION

Supplemental information can be found online at https://doi.org/10.1016/j.isci.2021.102071.

ACKNOWLEDGMENTS

We thank Ana Senra and Jose Malagón, at the University of Santiago de Compostela, for their technical support. We thank Prof Juan Zalvide for providing Rab-7 antibody. MGN is recipient of "Juan de la Cierva-Incorporación" fellowship (IJCI-2017-32606) from Ministerio de Ciencia, Innovación y Universidades, Spain. This work has been supported by grants from FEDER/Ministerio de Ciencia, Innovación y Universidades-Agencia Estatal de Investigación (CD: BFU2017-87721; RN: RTI2018-099413-B-I00). Financial support from the Xunta de Galicia (Centro singular de investigación de Galicia accreditation 2019-2022-ED431G 2019/02) and the European Union (European Regional Development Fund - ERDF) is gratefully acknowledged. The research leading to these results has also received funding from Xunta de Galicia 2015-CP080 and 2016-PG057 (RN). Centro de Investigación Biomédica en Red (CIBER) de Fisiopatología de la Obesidad y Nutrición (CIBERobn) is an initiative of the Instituto de Salud Carlos III (ISCIII) of Spain, which is supported by ERDF funds. MAFR is supported by the TALENTO Program by the Regional Madrid Government (2016/T1-BIO-1854).

AUTHOR CONTRIBUTIONS

Conceptualization: MGN and ARP. Methodology: MGN and ARP. Investigation: MGN, SBB, MD, CI, MGV, RA, NSL, and ARP. Data curation: MGN, SBB and ARP. Writing-Original Draft: MGN, CD and ARP. Writing-Review and Editing: MGN, SBB, RN, MAFR, CD and ARP. Funding Acquisition: RN, MAFR and CD. Supervision: MGN and ARP. All authors reviewed the final manuscript and agreed with the content.

DECLARATION OF INTERESTS

The authors declare no competing interests.

Received: September 25, 2020
Revised: December 14, 2020
Accepted: January 13, 2021
Published: February 19, 2021

REFERENCES

Balakrishnan, M., Patel, P., Dunn-Valadez, S., Dao, C., Khan, V., Ali, H., El-Serag, L., Hernaez, R., Sisson, A., Thrift, A.P., et al. (2020). Women have a lower risk of nonalcoholic fatty liver disease but a higher risk of progression vs men: a systematic review and meta-analysis. Clin. Gastroenterol. Hepatol. *19*, 61–71.e15.

Basaranoglu, M., Basaranoglu, G., Sabuncu, T., and Senturk, H. (2013). Fructose as a key player in the development of fatty liver disease. World J. Gastroenterol. *19*, 1166–1172.

Bates, J., Vijayakumar, A., Ghoshal, S., Marchand, B., Yi, S., Kornyeyev, D., Zagorska, A., Hollenback, D., Walker, K., Liu, K., et al. (2020). Acetyl-CoA carboxylase inhibition disrupts metabolic reprogramming during hepatic stellate cell activation. J. Hepatol. *73*, 896–905.

Browning, J.D., and Horton, J.D. (2004). Molecular mediators of hepatic steatosis and liver injury. J. Clin. Invest. *114*, 147–152.

Chen, X., Zhang, F., Gong, Q., Cui, A., Zhuo, S., Hu, Z., Han, Y., Gao, J., Sun, Y., Liu, Z., et al. (2016). Hepatic ATF6 increases fatty acid oxidation to attenuate hepatic steatosis in mice through peroxisome proliferator-activated receptor alpha. Diabetes *65*, 1904–1915.

Choi, Y., Abdelmegeed, M.A., and Song, B.J. (2017). Diet high in fructose promotes liver steatosis and hepatocyte apoptosis in C57BL/6J female mice: role of disturbed lipid homeostasis and increased oxidative stress. Food Chem. Toxicol. *103*, 111–121.

Chukijrungroat, N., Khamphaya, T., Weerachayaphorn, J., Songserm, T., and Saengsirisuwan, V. (2017). Hepatic FGF21 mediates sex differences in high-fat high-fructose diet-induced fatty liver. Am. J. Physiol. Endocrinol. Metab. *313*, E203–E212.

Cinaroglu, A., Gao, C., Imrie, D., and Sadler, K.C. (2011). Activating transcription factor 6 plays protective and pathological roles in steatosis due to endoplasmic reticulum stress in zebrafish. Hepatology *54*, 495–508.

Debosch, B.J., Chen, Z., Saben, J.L., Finck, B.N., and Moley, K.H. (2014). Glucose transporter 8 (GLUT8) mediates fructose-induced de novo lipogenesis and macrosteatosis. J. Biol. Chem. *289*, 10989–10998.

Diril, M.K., Schmidt, S., Krauss, M., Gawlik, V., Joost, H.G., Schurmann, A., Haucke, V., and Augustin, R. (2009). Lysosomal localization of GLUT8 in the testis–the EXXXLL motif of GLUT8 is sufficient for its intracellular sorting via AP1- and AP2-mediated interaction. FEBS J. *276*, 3729–3743.

DiStefano, J.K. (2020a). Fructose-mediated effects on gene expression and epigenetic mechanisms associated with NAFLD pathogenesis. Cell. Mol. Life Sci. *77*, 2079–2090.

DiStefano, J.K. (2020b). NAFLD and NASH in postmenopausal women: implications for diagnosis and treatment. Endocrinology *161*, bqaa134.

Du, T., Sun, X., Yuan, G., Zhou, X., Lu, H., Lin, X., and Yu, X. (2017). Sex differences in the impact of nonalcoholic fatty liver disease on cardiovascular risk factors. Nutr. Metab. Cardiovasc. Dis. *27*, 63–69.

Ganz, M., Csak, T., and Szabo, G. (2014). High fat diet feeding results in gender specific steatohepatitis and inflammasome activation. World J. Gastroenterol. *20*, 8525–8534.

Gasparin, F.R.S., Carreno, F.O., Mewes, J.M., Gilglioni, E.H., Pagadigorria, C.L.S., Natali, M.R.M., Utsunomiya, K.S., Constantin, R.P., Ouchida, A.T., Curti, C., et al. (2018). Sex differences in the development of hepatic steatosis in cafeteria diet-induced obesity in young mice. Biochim. Biophys. Acta Mol. Basis Dis. *1864*, 2495–2509.

Guo, B., and Li, Z. (2014). Endoplasmic reticulum stress in hepatic steatosis and inflammatory bowel diseases. Front. Genet. *5*, 242.

Hannou, S.A., Haslam, D.E., McKeown, N.M., and Herman, M.A. (2018). Fructose metabolism and metabolic disease. J. Clin. Invest. *128*, 545–555.

Hyer, M.M., Dyer, S.K., Kloster, A., Adrees, A., Taetzsch, T., Feaster, J., Valdez, G., and Neigh, G.N. (2019). Sex modifies the consequences of

extended fructose consumption on liver health, motor function, and physiological damage in rats. Am. J. Physiol. Regul. Integr. Comp. Physiol. *317*, R903–R911.

Ichiha, K., Kushunose, E., and Kusunose, M. (1969). Some properties and distribution of the omega-hydroxylation system of medium-chain fatty acids. Biochim. Biophys. Acta *176*, 704–712.

Jegatheesan, P., and De Bandt, J.P. (2017). Fructose and NAFLD: the multifaceted aspects of fructose metabolism. Nutrients *9*, 230.

Jensen, T., Abdelmalek, M.F., Sullivan, S., Nadeau, K.J., Green, M., Roncal, C., Nakagawa, T., Kuwabara, M., Sato, Y., Kang, D.H., et al. (2018). Fructose and sugar: a major mediator of non-alcoholic fatty liver disease. J. Hepatol. *68*, 1063–1075.

Kang, Y., and Kim, J. (2017). Soft drink consumption is associated with increased incidence of the metabolic syndrome only in women. Br. J. Nutr. *117*, 315–324.

Koyama, Y., and Brenner, D.A. (2017). Liver inflammation and fibrosis. J. Clin. Invest. *127*, 55–64.

Lau, J.K., Zhang, X., and Yu, J. (2017). Animal models of non-alcoholic fatty liver disease: current perspectives and recent advances. J. Pathol. *241*, 36–44.

Lonardo, A., Nascimbeni, F., Ballestri, S., Fairweather, D., Win, S., Than, T.A., Abdelmalek, M.F., and Suzuki, A. (2019). Sex differences in nonalcoholic fatty liver disease: state of the art and identification of research gaps. Hepatology *70*, 1457–1469.

Low, W.S., Cornfield, T., Charlton, C.A., Tomlinson, J.W., and Hodson, L. (2018). Sex differences in hepatic de novo lipogenesis with acute fructose feeding. Nutrients *10*, 1263.

Malhi, H., and Kaufman, R.J. (2011). Endoplasmic reticulum stress in liver disease. J. Hepatol. *54*, 795–809.

Miura, Y. (2013). The biological significance of omega-oxidation of fatty acids. Proc. Jpn. Acad. Ser. B Phys. Biol. Sci. *89*, 370–382.

Mortensen, P.B. (1980). The possible antiketogenic and gluconeogenic effect of the omega-oxidation of fatty acids in rats. Biochim. Biophys. Acta *620*, 177–185.

Rodgers, M., Heineman, B., and Dushay, J. (2019). Increased fructose consumption has sex-specific effects on fibroblast growth factor 21 levels in humans. Obes. Sci. Pract. *5*, 503–510.

Schmidt, S., Joost, H.G., and Schurmann, A. (2009). GLUT8, the enigmatic intracellular hexose transporter. Am. J. Physiol. Endocrinol. Metab. *296*, E614–E618.

Schuck, R.N., Zha, W., Edin, M.L., Gruzdev, A., Vendrov, K.C., Miller, T.M., Xu, Z., Lih, F.B., DeGraff, L.M., Tomer, K.B., et al. (2014). The cytochrome P450 epoxygenase pathway regulates the hepatic inflammatory response in fatty liver disease. PLoS One *9*, e110162.

Spruss, A., Henkel, J., Kanuri, G., Blank, D., Puschel, G.P., Bischoff, S.C., and Bergheim, I. (2012). Female mice are more susceptible to nonalcoholic fatty liver disease: sex-specific regulation of the hepatic AMP-activated protein kinase-plasminogen activator inhibitor 1 cascade, but not the hepatic endotoxin response. Mol. Med. *18*, 1346–1355.

Ter Horst, K.W., and Serlie, M.J. (2017). Fructose consumption, lipogenesis, and non-alcoholic fatty liver disease. Nutrients *9*, 981.

Todoric, J., Di Caro, G., Reibe, S., Henstridge, D.C., Green, C.R., Vrbanac, A., Ceteci, F., Conche, C., McNulty, R., Shalapour, S., et al. (2020). Fructose stimulated de novo lipogenesis is promoted by inflammation. Nat. Metab. *2*, 1034–1045.

Van Herck, M.A., Vonghia, L., and Francque, S.M. (2017). Animal models of nonalcoholic fatty liver disease-A starter's guide. Nutrients *9*, 1072.

Vila, L., Roglans, N., Perna, V., Sanchez, R.M., Vazquez-Carrera, M., Alegret, M., and Laguna, J.C. (2011). Liver AMP/ATP ratio and fructokinase expression are related to gender differences in AMPK activity and glucose intolerance in rats ingesting liquid fructose. J. Nutr. Biochem. *22*, 741–751.

Vos, M.B., and Lavine, J.E. (2013). Dietary fructose in nonalcoholic fatty liver disease. Hepatology *57*, 2525–2531.

Wanders, R.J., Komen, J., and Kemp, S. (2011). Fatty acid omega-oxidation as a rescue pathway for fatty acid oxidation disorders in humans. FEBS J. *278*, 182–194.

Wen, A.Y., Sakamoto, K.M., and Miller, L.S. (2010). The role of the transcription factor CREB in immune function. J. Immunol. *185*, 6413–6419.

Yang, M., Liu, Q., Huang, T., Tan, W., Qu, L., Chen, T., Pan, H., Chen, L., Liu, J., Wong, C.W., et al. (2020). Dysfunction of estrogen-related receptor alpha-dependent hepatic VLDL secretion contributes to sex disparity in NAFLD/NASH development. Theranostics *10*, 10874–10891.

Zeng, L., Lu, M., Mori, K., Luo, S., Lee, A.S., Zhu, Y., and Shyy, J.Y. (2004). ATF6 modulates SREBP2-mediated lipogenesis. EMBO J. *23*, 950–958.

Zhong, F., Zhou, X., Xu, J., and Gao, L. (2020). Rodent models of nonalcoholic fatty liver disease. Digestion *101*, 522–535.

iScience, Volume *24*

Supplemental Information

Impact of liver-specific GLUT8 silencing on fructose-induced inflammation and omega oxidation

Marta G. Novelle, Susana Belén Bravo, Maxime Deshons, Cristina Iglesias, María García-Vence, Rebecca Annells, Natália da Silva Lima, Rubén Nogueiras, Manuel Alejandro Fernández-Rojo, Carlos Diéguez, and Amparo Romero-Picó

Figure S1

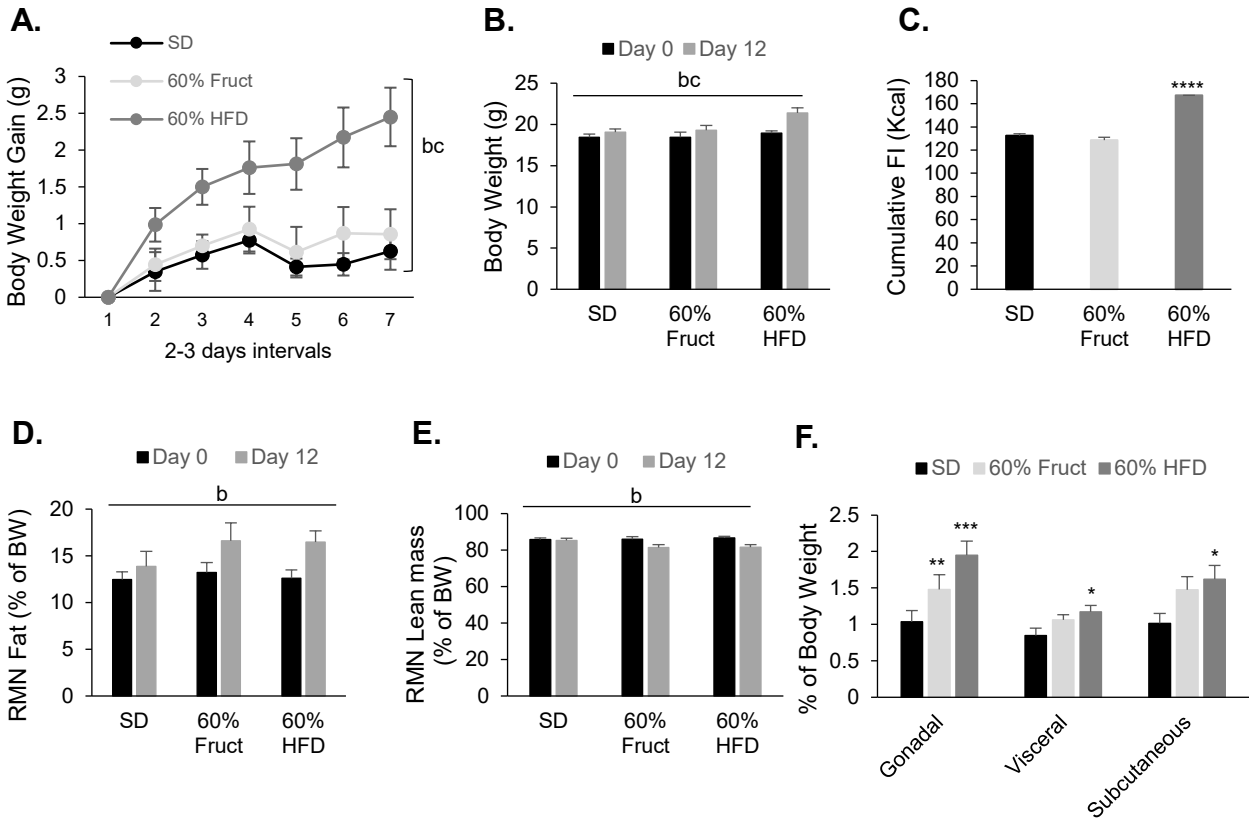
A.
SD
60% Fructose
60% HFD
Body Weight Gain (g)
bc
2-3 days intervals
B.
Day 0
Day 12
bc
Body Weight (g)
SD
60% Fructose
60% HFD
C.
Cumulative FI (Kcal)
****
SD
60% Fructose
60% HFD
D.
Day 0
Day 12
b
RMN Fat (% of BW)
SD
60% Fructose
60% HFD
E.
Day 0
Day 12
b
RMN Lean mass (% of BW)
SD
60% Fructose
60% HFD
F.
SD
60% Fructose
60% HFD
% of Body Weight
Gonadal
Visceral
Subcutaneous

Figure S2

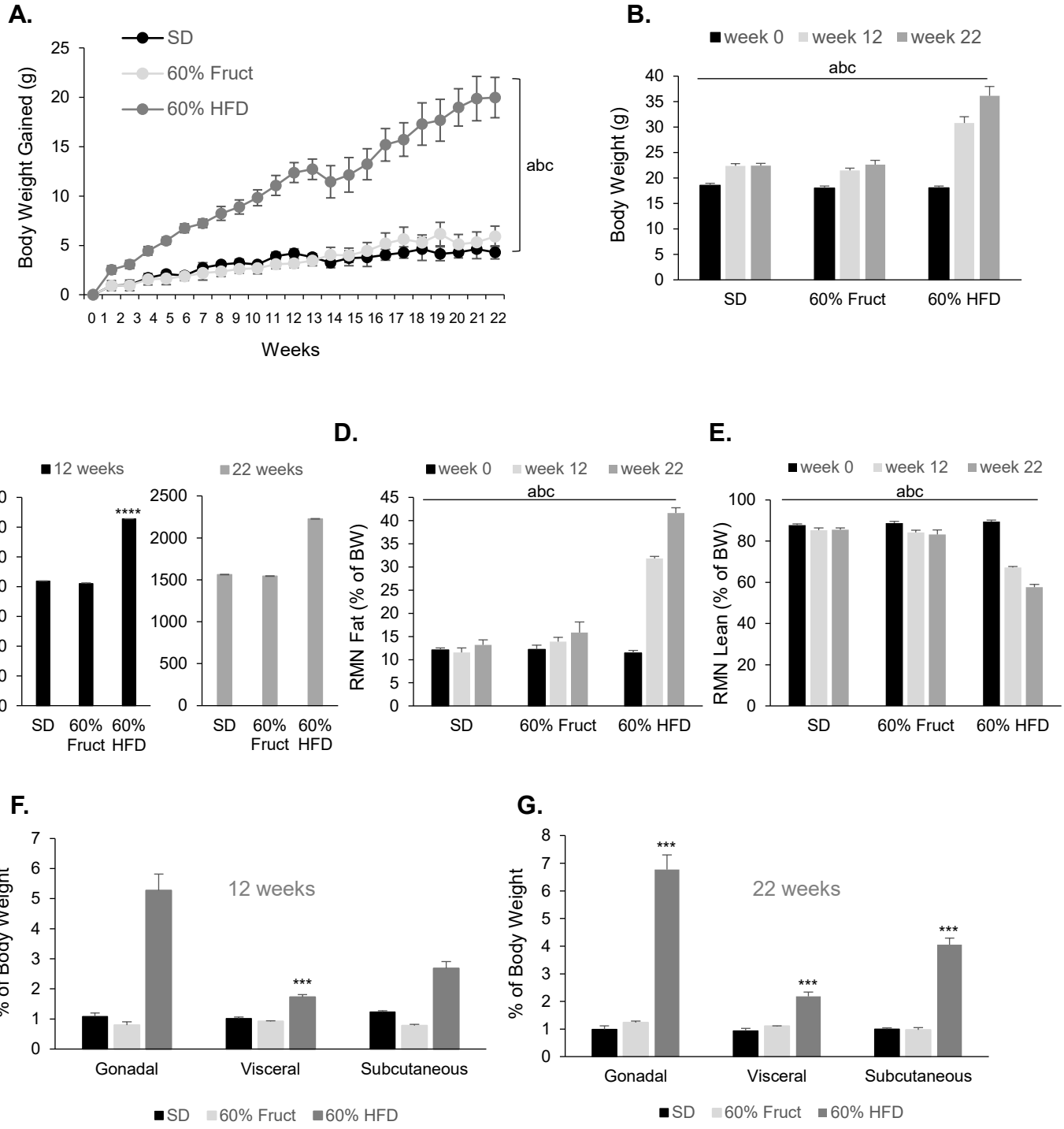
A.
SD
60% Fruct
60% HFD
Body Weight Gained (g)
Weeks
abc
B.
week 0
week 12
week 22
abc
Body Weight (g)
SD
60% Fruct
60% HFD
C.
12 weeks
22 weeks
Cumulative FI (Kcal)
****
SD
60% Fruct
60% HFD
D.
week 0
week 12
week 22
abc
RMN Fat (% of BW)
SD
60% Fruct
60% HFD
E.
week 0
week 12
week 22
abc
RMN Lean (% of BW)
SD
60% Fruct
60% HFD
F.
12 weeks
% of Body Weight
***
Gonadal
Visceral
Subcutaneous
SD
60% Fruct
60% HFD
G.
22 weeks
% of Body Weight
***
***
***
Gonadal
Visceral
Subcutaneous
SD
60% Fruct
60% HFD

Figure S3

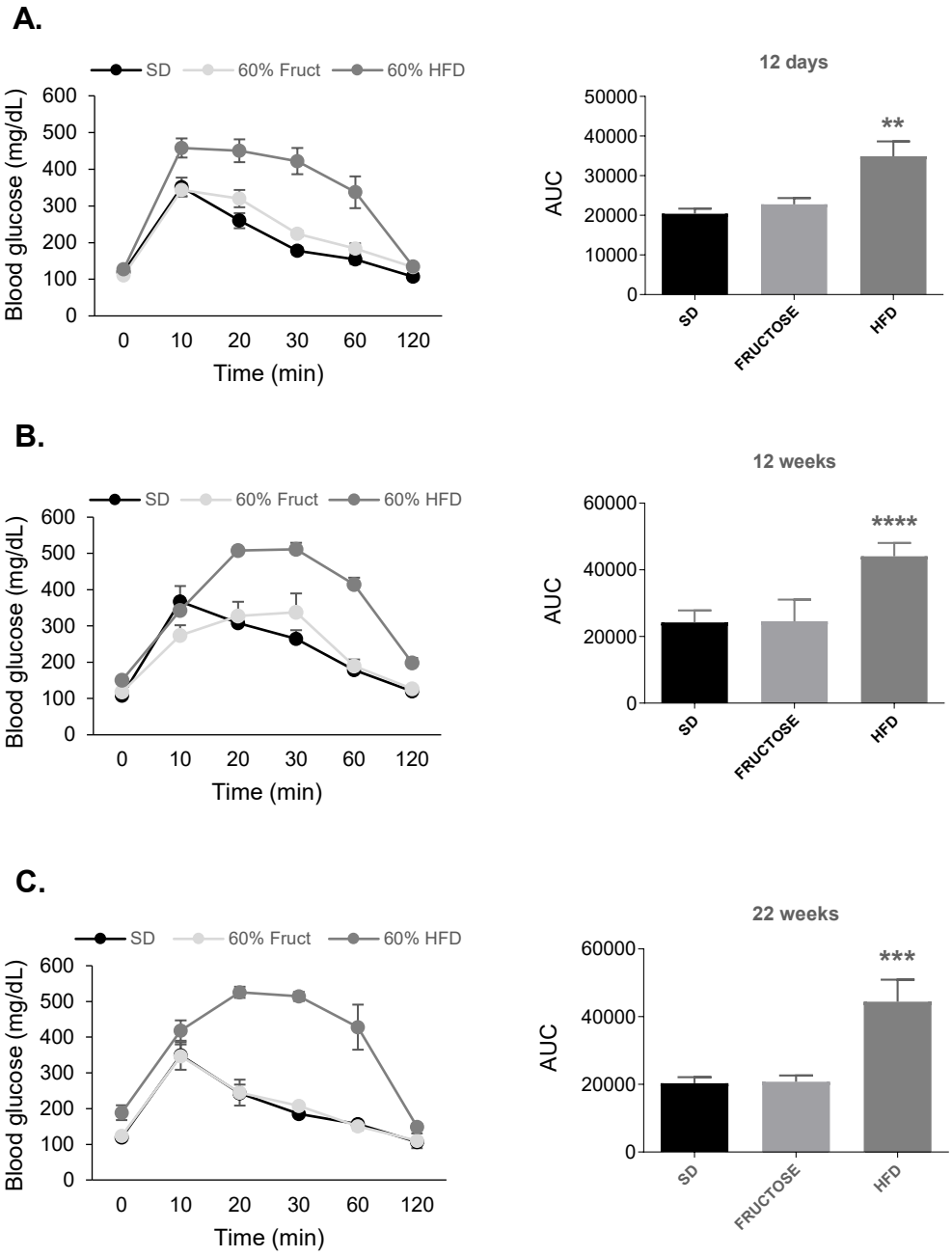
A.
SD
60% Fruct
60% HFD
Blood glucose (mg/dL)
600
500
400
300
200
100
0
0
10
20
30
60
120
Time (min)
12 days
AUC
50000
40000
30000
20000
10000
0
**
SD
FRUCTOSE
HFD
B.
SD
60% Fruct
60% HFD
Blood glucose (mg/dL)
600
500
400
300
200
100
0
0
10
20
30
60
120
Time (min)
12 weeks
AUC
60000
40000
20000
0
****
SD
FRUCTOSE
HFD
C.
SD
60% Fruct
60% HFD
Blood glucose (mg/dL)
600
500
400
300
200
100
0
0
10
20
30
60
120
Time (min)
22 weeks
AUC
60000
40000
20000
0
***
SD
FRUCTOSE
HFD

Figure S4

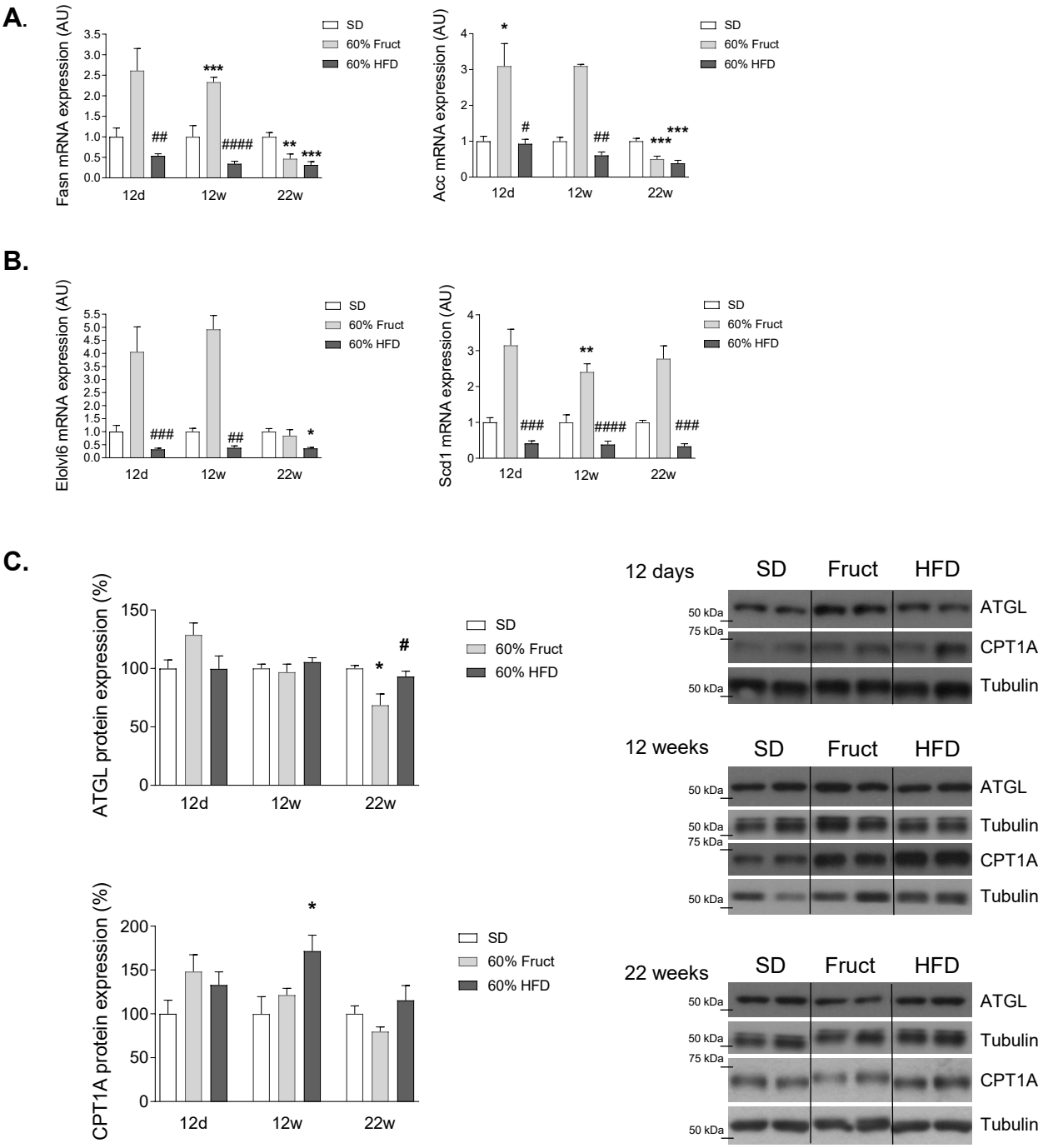
A.
Fasn mRNA expression (AU)
SD
60% Fruct
60% HFD
12d
12w
22w
Acc mRNA expression (AU)
B.
Elovl6 mRNA expression (AU)
Scd1 mRNA expression (AU)
C.
ATGL protein expression (%)
CPT1A protein expression (%)
12 days
12 weeks
22 weeks
SD
Fruct
HFD
50 kDa
75 kDa
ATGL
CPT1A
Tubulin

Figure S5

A.

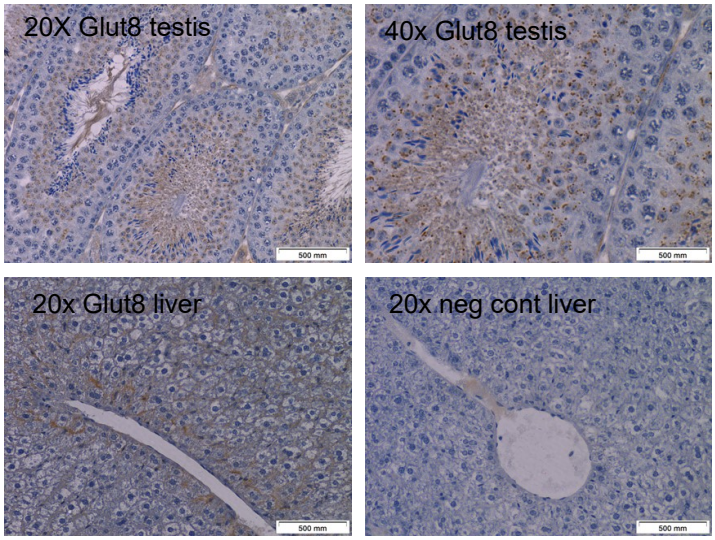
20X Glut8 testis
40x Glut8 testis
20x Glut8 liver
20x neg cont liver
500 mm
500 mm
500 mm
500 mm

Figure S6

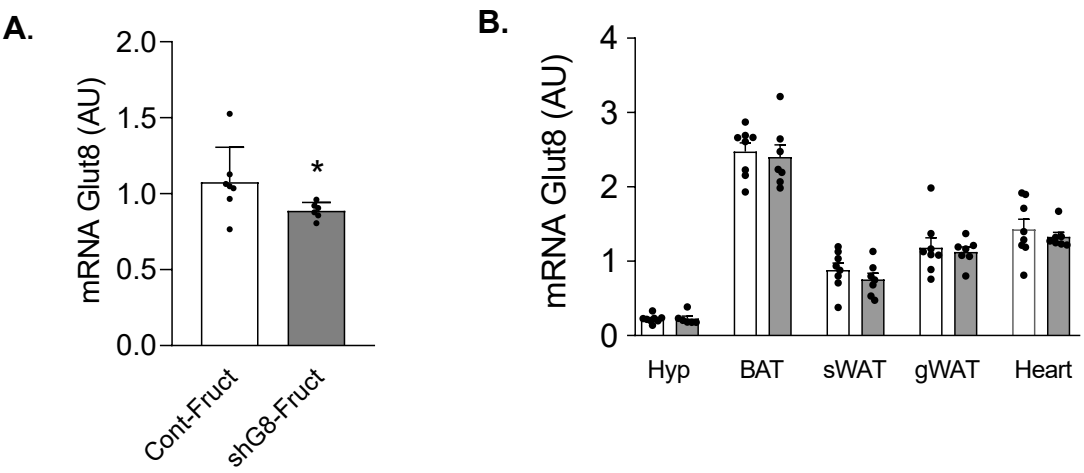
A.
mRNA Glut8 (AU)
2.0
1.5
1.0
0.5
0.0
*
Cont-Fruct
shG8-Fruct
B.
mRNA Glut8 (AU)
4
3
2
1
0
Hyp
BAT
sWAT
gWAT
Heart

Figure S7.

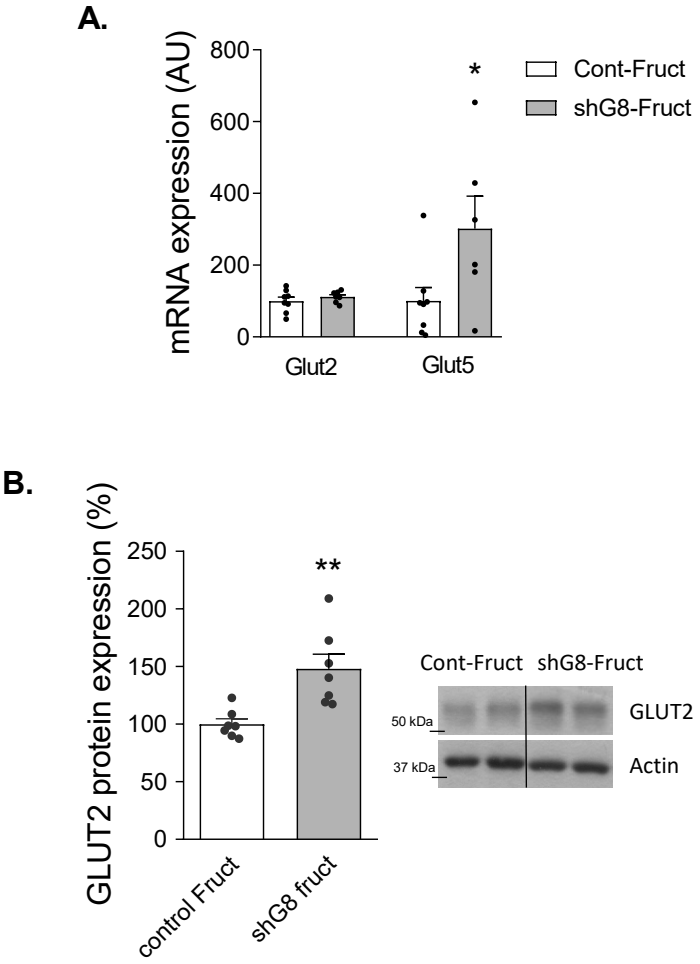
A.
mRNA expression (AU)
800
600
400
200
0
*
Cont-Fruct
shG8-Fruct
Glut2
Glut5
B.
GLUT2 protein expression (%)
250
200
150
100
50
0
**
control Fruct
shG8 fruct
Cont-Fruct
shG8-Fruct
50 kDa
37 kDa
GLUT2
Actin

Figure S8

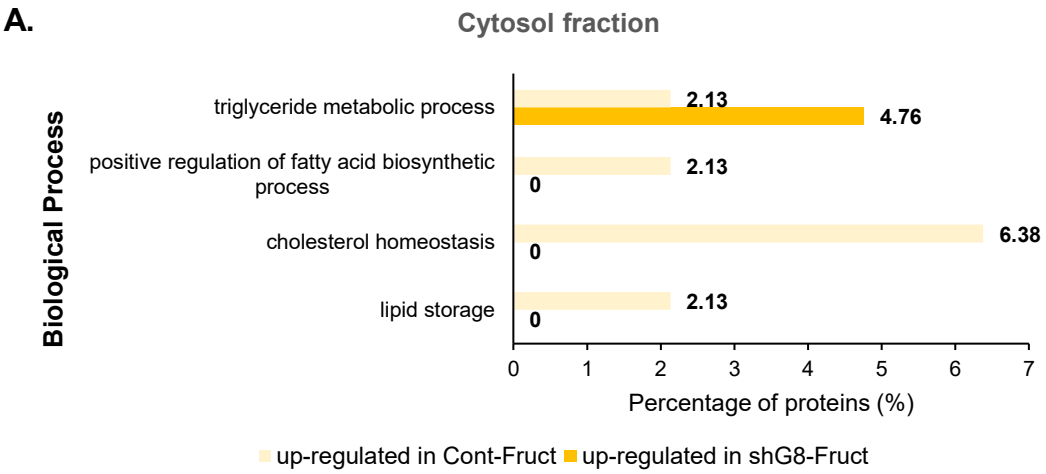
A.
Cytosol fraction
Biological Process
triglyceride metabolic process
positive regulation of fatty acid biosynthetic process
cholesterol homeostasis
lipid storage
2.13
4.76
2.13
0
6.38
0
2.13
0
0 1 2 3 4 5 6 7
Percentage of proteins (%)
up-regulated in Cont-Fruct
up-regulated in shG8-Fruct

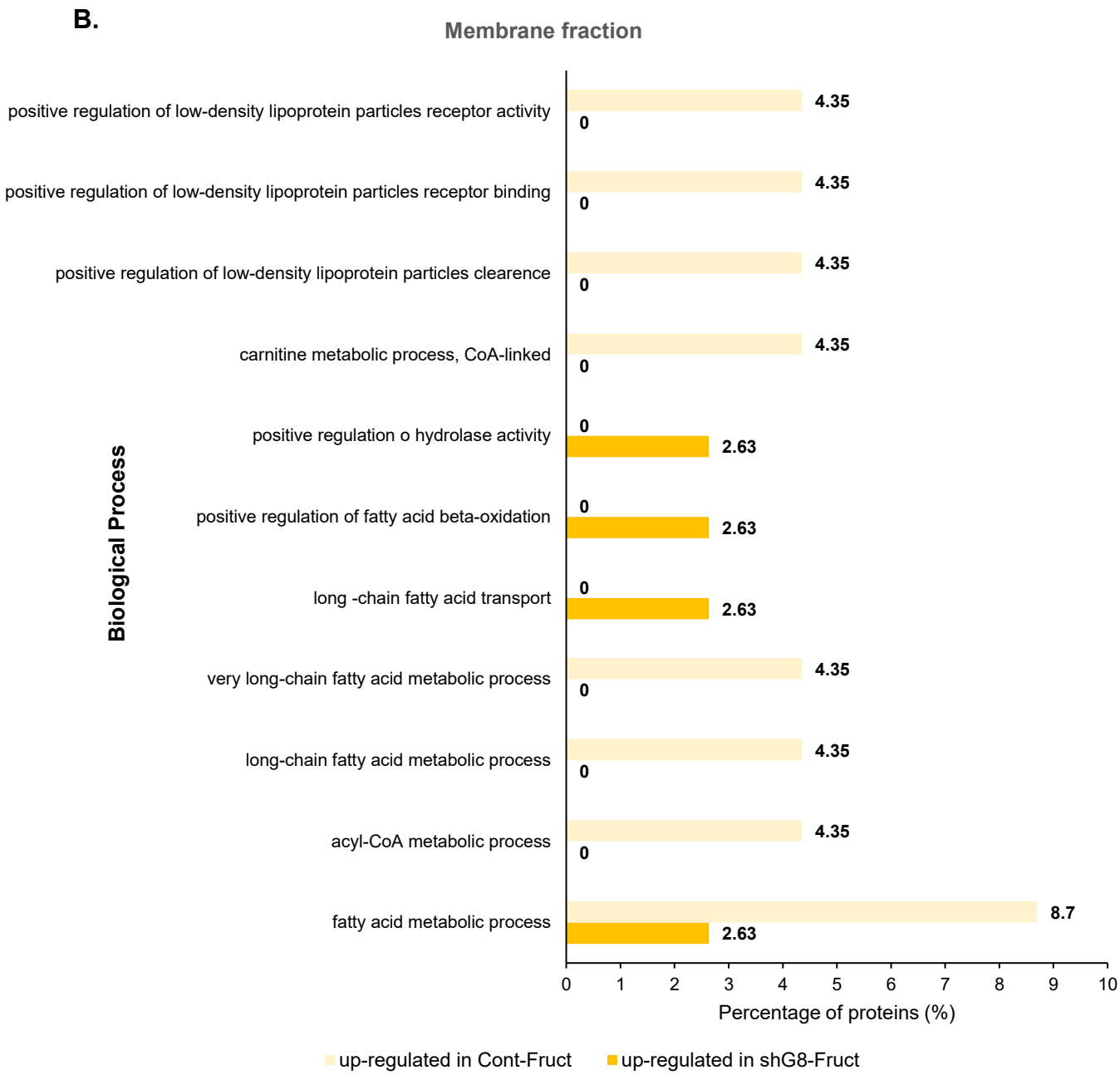
B.
Membrane fraction
Biological Process
positive regulation of low-density lipoprotein particles receptor activity
positive regulation of low-density lipoprotein particles receptor binding
positive regulation of low-density lipoprotein particles clearence
carnitine metabolic process, CoA-linked
positive regulation o hydrolase activity
positive regulation of fatty acid beta-oxidation
long -chain fatty acid transport
very long-chain fatty acid metabolic process
long-chain fatty acid metabolic process
acyl-CoA metabolic process
fatty acid metabolic process
4.35
0
4.35
0
4.35
0
4.35
0
0
2.63
0
2.63
0
2.63
4.35
0
4.35
0
4.35
0
8.7
2.63
0 1 2 3 4 5 6 7 8 9 10
Percentage of proteins (%)
up-regulated in Cont-Fruct
up-regulated in shG8-Fruct

Figure S9.

A.

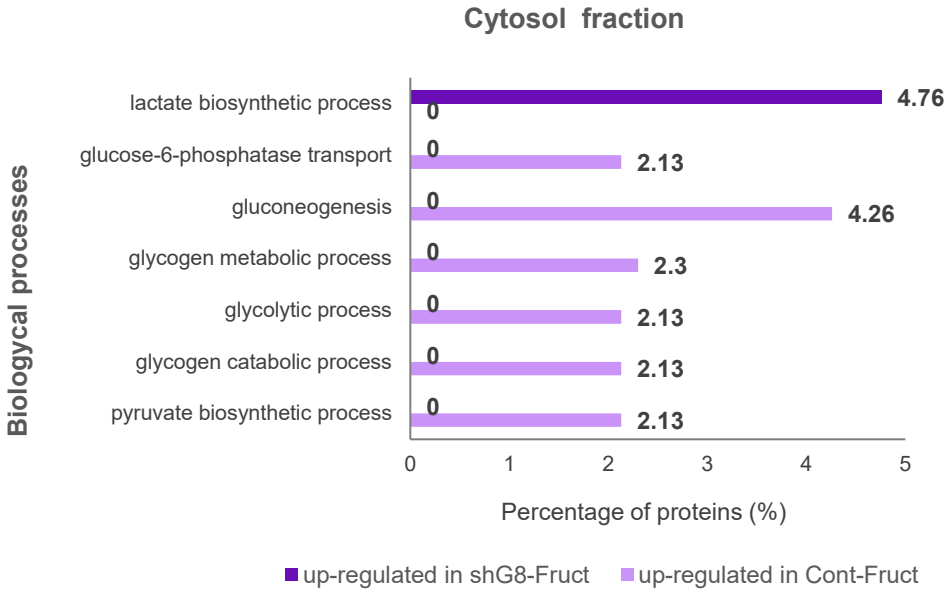
Cytosol fraction
Biologycal processes
lactate biosynthetic process
glucose-6-phosphatase transport
gluconeogenesis
glycogen metabolic process
glycolytic process
glycogen catabolic process
pyruvate biosynthetic process
0
4.76
0
2.13
0
4.26
0
2.3
0
2.13
0
2.13
0
2.13
0 1 2 3 4 5
Percentage of proteins (%)
up-regulated in shG8-Fruct
up-regulated in Cont-Fruct

B.

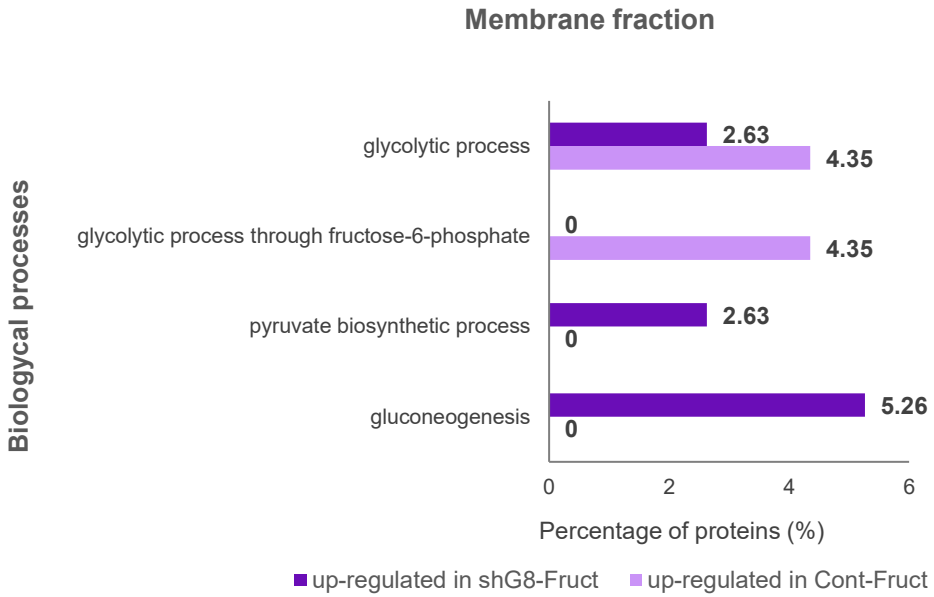
Membrane fraction
Biologycal processes
glycolytic process
glycolytic process through fructose-6-phosphate
pyruvate biosynthetic process
gluconeogenesis
2.63
4.35
0
4.35
2.63
0
5.26
0
0 2 4 6
Percentage of proteins (%)
up-regulated in shG8-Fruct
up-regulated in Cont-Fruct

Figure S10.

A.

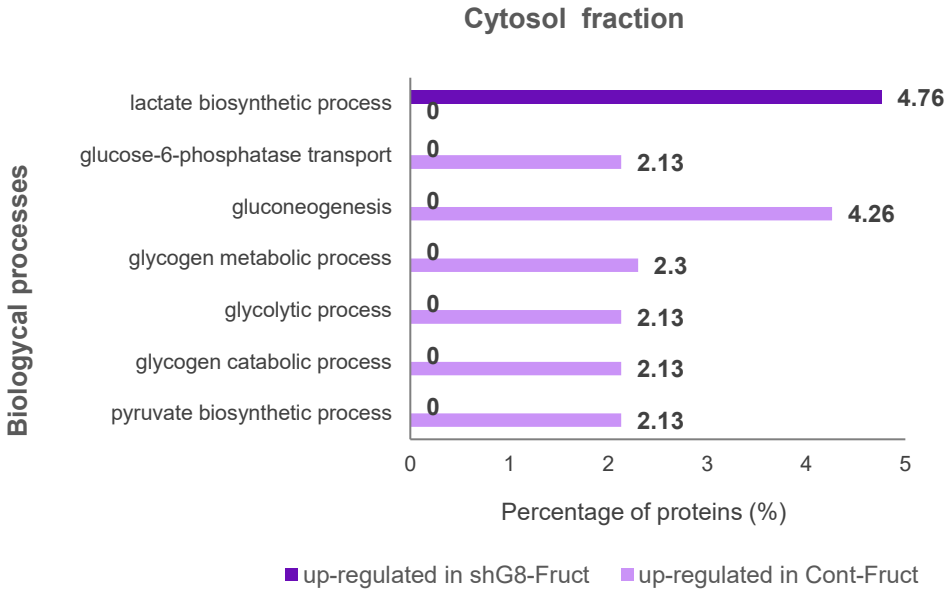

B.

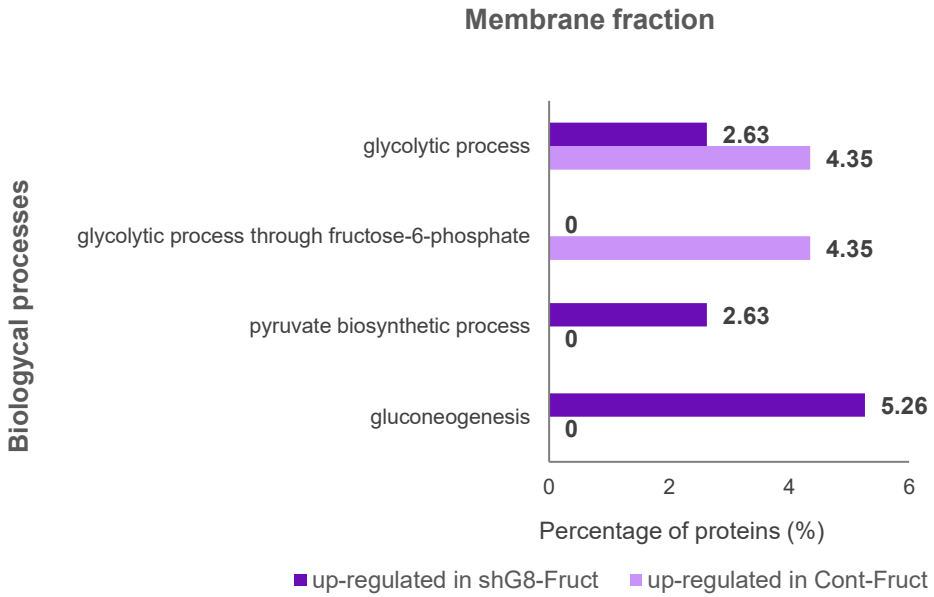

Figure S11

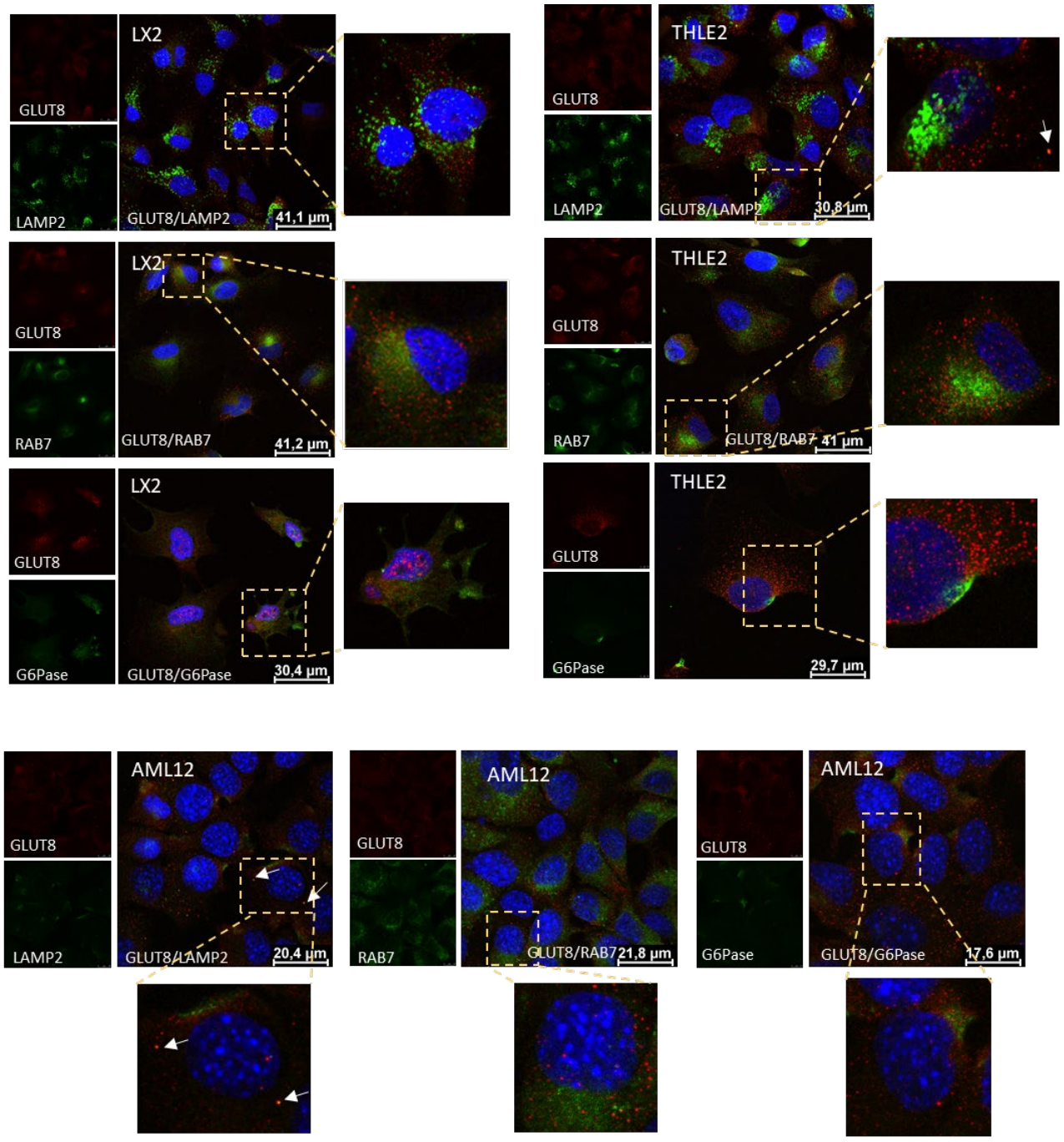
GLUT8
LAMP2
LX2
GLUT8/LAMP2
41,1 µm
GLUT8
LAMP2
THLE2
GLUT8/LAMP2
30,8 µm
GLUT8
RAB7
LX2
GLUT8/RAB7
41,2 µm
GLUT8
RAB7
THLE2
GLUT8/RAB7
41 µm
GLUT8
G6Pase
LX2
GLUT8/G6Pase
30,4 µm
GLUT8
G6Pase
THLE2
29,7 µm
GLUT8
LAMP2
AML12
GLUT8/LAMP2
20,4 µm
GLUT8
RAB7
AML12
GLUT8/RAB7
21,8 µm
GLUT8
G6Pase
AML12
GLUT8/G6Pase
17,6 µm

Supplemental Figure Legends

Figure S1. Related to Figure 1. Metabolic characterisation of female mice under short-term diet exposure. (A) Evolution of body weight gain and (B) initial versus final weight were determined in animals subjected to SD, Fructose diet and HFD. (C) Cumulative food intake (FI) expressed as Kcal ingested was recorded after 12 days. (D) Percentage of fat content and (E) lean mass analysed by EchoMRI and (F) measurement of the main fat depots. Results are expressed as mean ± SEM. 12 days (n=8 mice per group), 12 weeks (n=4 mice per group), and 22 weeks (n=4 mice per group). One way-ANOVA *p≤0.05, **p≤0.01, *** p≤0.001; (* compared to SD) or two-way ANOVA (diet, time) were conducted. a=diet effect, b=time effect, c=significant interaction.

Figure S2. Related to Figure 1. Metabolic characterisation of female mice under long-term diet exposure. (A) Evolution of body weight gain and (B) initial versus final weight were determined in animals subjected to SD, Fructose diet and HFD. (C) Cumulative food intake (FI) expressed as Kcal ingested was recorded after 12 weeks and 22 weeks. (D) Percentage of fat content and (E) lean mass analysed by EchoMRI and (F) measurement of the main fat depots at 12 weeks and (G) 22 weeks. Results are expressed as mean ± SEM. 12 days (n=8 mice per group), 12 weeks (n=4 mice per group), and 22 weeks (n=4 mice per group). One way-ANOVA *p≤0.05, **p≤0.01, *** p≤0.001; (* compared to SD) or two-way ANOVA (diet, time) were conducted. a=diet effect, b=time effect, c=significant interaction.

Figure S3. Related to Figure 1. HFD modifies the glucose tolerance of female mice after 12 days, 12 weeks and 22 weeks of diet. Blood glucose levels during ipGTT performed in 6-h fasted mice at 12 days (A), 12 weeks (B) and 22 weeks (C) (AUC shown on the right). Results are expressed as mean ± SEM. 12 days (n=8 mice per group), 12 weeks (n=4 mice per group), and 22 weeks (n=4 mice per group). One way-ANOVA *p≤0.05, **p≤0.01, *** p≤0.001; (* compared to SD).

Figure S4. Related to Figure 1. Fructose diet and HFD modify lipogenic and lipolytic hepatic pathways. (A) Genetic expression of lipogenic cytosolic enzymes Fasn and Acc, and (B) the lipogenic intramembrane enzymes Elovl6 that catalyses the conversion of palmitate to stearate, and Scd1 the rate-limiting enzyme that converts saturated fatty acids (SFAs) to monounsaturated fatty acids (MUFAs), at different time points in female mice subjected to SD, fructose diet and HFD. (C) Protein expression of lipolytic enzymes ATGL and CPT1A at different time points in female mice subjected to SD, fructose diet and HFD. Representative images of blots are shown. Dividing lines indicate splicing in the same gel. Results are expressed as mean ± SEM. 12 days (n=8 mice per group), 12 weeks (n=4 mice per group), and 22 weeks (n=4 mice per group). One-Way ANOVA and Post Hoc Test (* compared to SD, # compared to 60% Fructose). *p≤0.05, **p≤0.01, *** p≤0.001.

Figure S5. Related to Figure 3. (A) Validation of the specificity of GLUT8 antibody by immunohistochemistry analysis using mouse testis as a positive control. Sections were photographed using a BX51 microscope equipped with a DP70 digital camera (Olympus).

Figure S6. Related to Figure 3. GLUT8 was specifically downregulated within the liver in high-fructose fed animals for 22 weeks. (A) Genetic expression of Glut8 in the mice livers. (B) Genetic expression of Glut8 in different tissues metabolically active (hypothalamus, brown adipose tissue, subcutaneous white adipose tissue, gonadal adipose tissue and heart). Results are expressed as mean ± SEM. n=7-8 mice per group. T-test or Mann-Whitney test were conducted. *p≤0.05, **p≤0.01, *** p≤0.001.

Figure S7. Related to Figure 3. Other fructose transporters were upregulated when silencing Glut8 within the liver in high-fructose fed animals for 22 weeks. (A) Genetic expression of Glut2 and Glut5 in the mice livers. (B) GLUT2 protein expression in the liver after Glut8 silencing. Representative images of blots are shown. Dividing lines indicate splicing in the same gel. Results are expressed as mean ± SEM. n=6-8 mice per group. T-test or Mann-Whitney test were conducted. *p≤0.05, **p≤0.01, *** p≤0.001.

Figure S8. Related to Figure 4. Percentage of proteins implicated in different biological processes. Up-regulated proteins in the control-fructose group (n=4 samples) are shown in light yellow both cytosol and membrane fraction. Up-regulated proteins in the sh-GLUT8-fructose group (n=4 samples) are shown in dark yellow.

Figure S9. Related to Figure 4. Percentage of proteins related with glucose metabolism in cytosol fraction (A) and membrane fraction (B). Up-regulated proteins in the sh-GLUT8-fructose group (n=4 samples) both in membrane and cytosolic fractions are shown in dark colours. Up-regulated proteins in the control-fructose group (n=4 samples) are shown in light colours.

Figure S10. Related to Figure 4. Percentage of proteins related with oxidative stress (A) and ER stress (B) processes. Up-regulated proteins in the sh-GLUT8-fructose group (n=4 samples) both in membrane and cytosolic fractions are shown in dark colours (A, green; B, brown). Up-regulated proteins in the control-fructose group (n=4 samples) are shown in light colours.

Figure S11. Related to Figure 6-7. Studying of colocalization of GLUT8 (shown in red) with LAMP2 (a marker of lysosomes), Rab7 (a marker of late endosomes) or G6Pase (a marker of ER/microsomes) (shown in green) in (A) the LX-2 human hepatic stellate cell line, (B) the THLE2 human hepatocytes cells line and (C) the AML12 murine hepatocytes cell line. Colocalization from merge is shown in yellow (white arrows). Images were photographed using the Confocal Espectral Leica AOBS-SP5.

Transparent methods

Animal procedures and diets

C57BL/6 adult female mice (8 weeks old) were housed individually and maintained on a 12:12-h light-dark cycle. They were allowed *ad libitum* access to water and food. Energy value of the diets used in this study was: standard chow diet (SD) (Safe A04, in which 72.3 % of calories are from carbohydrates, 8.4% from lipids, 19.3% from proteins; totalling 3.34 Kcal g^{-1}) purchased from Panlab (Spain); high-fructose diet (D02022704, in which 70% of calories are from carbohydrates which 60% are from fructose, 10% from fat, 20% from proteins; totalling 3.85 Kcal g^{-1}), and high-fat diet (HFD) (D12492, in which 20% of calories are from carbohydrates, 60% from fat, 20% from proteins; totalling 5.21 Kcal g^{-1}) purchased from Research Diets (USA). All animal procedures were conducted in accordance with the standards approved by the Animal Ethics Committee (AEC) at the University of Santiago de Compostela, and experiments were performed following the Animal Research Reporting of In Vivo Experiments (ARRIVE) guidelines and in agreement with the rules of Laboratory Animal Care and International Law on Animal Experimentation.

Experimental setting 1: Effect of 60% fructose and 60% high-fat diets compared to standard diet.
Adult C57BL/6 female mice were grouped and feed *ad libitum* with 1) SD, 2) 60% Fructose, and 3) 60% HFD, at different time points (n=4-8 per group): 12 days (short- term), 12 weeks (medium-term), and 22 weeks (long-term). Body weight and food intake were monitored once *per* week. Glucose tolerance tests (GTT) were performed and mice were subjected to NMR imaging to determinate body composition. Animals were killed by decapitation. Liver and serum were collected and frozen at -80ºC.

Experimental setting 2: Effect of specific liver GLUT8 inhibition over long term consumption of rich fructose diet.
$1x10^6$ TU/mL lentiviral particles (SIGMA) containing a vector PLO.1-CMV-tGFP encoding for shRNA against murine Glut8 (shG8-Fruct) or null shRNA (Cont-Fruct) were delivered by tail vein injection to 8-week-old C57BL/6 female mice. From the day of injection, they were allowed *ad libitum* access to a 60% fructose diet for 22 weeks. Body weight and food intake were monitored once *per* week. At 22 weeks animals were killed by decapitation. Tissues (liver, BAT, subcutaneous and gonadal WAT, hypothalamus and heart) and serum were collected and frozen at -80ºC.

Determination of body composition

Whole body composition was measured using NMR imaging (Whole Body Composition Analyzer; EchoMRI, Houston, TX) (Novelle et al., 2017; Porteiro et al., 2018).

Glucose tolerance test

Mice were fasted for 6 h and then given an i.p. glucose load (2 g/ kg body weight) of a 20% glucose solution. Blood was sampled from the tail vein. Glucose levels were measured before glucose injection (0 minutes) and at different time points, using a Glucocard glucometer (A. Menarini diagnostics, Spain). The areas under the curve (AUC) were calculated from 0 to 120 minutes and baselines were set at the fasting levels (Tuduri et al., 2016).

Serum levels of metabolites

Whole trunk blood was collected and then spun for 15 minutes at 3000xg and 4°C. The supernatant was transferred to a new tube to obtain the serum. Serum cholesterol levels (1001093, Spinreact), triglycerides levels (1001310, Spinreact) and free fatty acids levels (436-91995, 434-91795, WAKO) were measured using commercial kits based on a colorimetric method by spectrophotometry in a ThermoScientific Multiskan GO spectrophotometer.

Liver TG and free fatty acids content

Livers (approx. 500 mg) were homogenized for 2 minutes in ice-cold chloroform-methanol (2:1, vol/vol). TG and free fatty acids were extracted during 3-h shaking at room temperature. For phase separation, milli-Q water was added, samples were centrifuged, and the organic bottom layer was collected. The organic solvent was dried using a Speed Vac and re-dissolved in

chloroform. Metabolite content of each sample was measured in duplicate after evaporation of the organic solvent using the enzymatic methods described above (Spinreact, Spain).

Cell culture

The LX-2 human hepatic stellate cell line (SCC064, MERCK) and murine AML-12 (ATCC CRL-2254) cells were maintained in DMEM/F12 containing 10% (v/v) FBS, 5% ITS (insulin/transferrin/selenium; SIGMA), and dexamethasone (DX) (0.4 µg/mL) (SIGMA). The THLE2 human hepatic cell line (ATCC CRL-2706) was grown in bronchial epithelial cell basal medium (BEBM; cc-3171, Lonza/Clonetics Corporation) supplemented with a growth factor BulleKit (cc-3170, Lonza/Clonetics Corporation), 70ng/mL phosphoethanolamine, 5 ng/mL epidermal growth factor, 10% (v/v) FBS and 1% (v/v) Glutamine-Penicillin-Streptomycin solution (MERCK). Cells were cultured at 37ºC in a humidified atmosphere containing 5% CO2.

Cell treatments

LX-2 and AML12 cells were seeded onto six-well plates for final confluence of 80-90%. After 24 h in culture, the initial medium was replaced for a fresh one according to the treatment requirements, as follows: SD, *"standard diet",* (DMEM 17mM glucose); Fructose diet, (25 mM fructose, SIGMA, in DMEM Low Glucose (5mM)); HFD *"high- fat diet"* (SD plus 500µM palmitic acid #P9767 SIGMA in ethanol and 500µM linoleic acid-oleic acid #L9655 SIGMA). All mediums were supplemented with 10% (v/v) FBS, 5% ITS and 0.4 µg/mL DX. After another 24 h, cells were collected for protein and RNA extraction and immunocytochemistry analysis.

Cell transfection

LX-2 and THLE2 cells were seeded onto six-well plates at an initial confluence of 40-50%. After 24 h in culture, cells were transfected with specific small-interfering RNA (si-RNA) to knock down the expression of GLUT8 (ON-TARGET plus human SLC2A8, Dharmacon™, USA). Non-targeting siRNA was used as a negative control (Dharmacon™). Cells were transfected using Dharmafect 1 reagent form Dharmacon™ following the protocol: 10 µL of each siRNA (5 µM) diluted in 190 µL of optiMEM (Life Technologies, USA), mixed with 6.5 µL of Dharmafect1 diluted in 193.5 µL of optiMEM (Life Technologies, USA). This mixture was incubated in a final volume of 2 mL of a complete specific medium during 24h. After silencing GLUT8, the medium was replaced with fresh high-fructose medium (25 mM fructose) for another 24 h until cells were collected for protein and RNA extraction and immunofluorescence and Oil Red analyses.

Histological procedures

Hepatic lipid content was analysed by Oil Red staining. Frozen sections of the livers (10 µm) were cut, fixed in 10% buffered formalin and stained in filtered Oil Red O (SIGMA O0625) for 10 min. Sections were washed in distilled water, counterstained with Harris's haematoxylin (Bio-Optica 05-06004/L) for 5 min and mounted in aqueous mounting (BioOptica 05-1740). Fresh liver samples were fixed in 10% buffered formalin for 24 h, and then dehydrated and embedded in paraffin by a standard procedure. Sections of 4 µm were cut with a microtome and stained using a standard Hematoxylin/Eosin Alcoholic procedure according to the manufacturer's instructions (BioOptica, Milan, Italy). Sections were then rinsed with distilled water, dried for 30 minutes at 37°C, and then mounted with permanent (non-alcohol, non-xylene based) mounting media. For Sirius Red staining, samples fixated in paraffin were dewaxed, hydrated and stained in PicroSirius staining red (SIGMA, 365548) for an hour. After two washes with acidified water, samples were dehydrated in three changes of 100% ethanol, cleared in xylene and mounted in a resinous medium. Sections were photographed using a BX51 microscope equipped with a DP70 digital camera (Olympus) and analysed using ImageJ software 1.43r (NIH, Bethesda).

Immunohistochemistry

For GLUT8 immunohistochemistry staining, samples fixated in paraffin were dewaxed, hydrated, pre-treated in PTLink TE buffer pH 6 and blocked with 3% peroxidase for 10 minutes. Sections

were then incubated with the primary antibody (Millipore 07-1407) at a concentration of 1:500 overnight at 4°C, followed by incubation with the secondary antibody for 30 minutes at room temperature. After that, DAB developer (DAKO-K3468) was used for 1 minute and the sections were counterstained with Mayer´s hematoxylin (Bio-Optica 1060021000) for 10 min, dehydrated and mounted. For GLUT8 immunocytochemistry LX2 and AML12 cells, coverslips were washed with PBS and fixed with 10% buffered formalin for 10 minutes. After that, cells were permeabilised with 0.2 % Triton X-100 in PBS before incubation with primary antibody. Negative controls without primary antibodies were included to assess non-specific staining.

Immunofluorescence

To visualize GLUT8 expression in intracellular organelles, LX2 and THLE2 cells were also fixed with 10% buffered formalin for 10 minutes and permeabilised with 0.2 % Triton X-100 in PBS. Subsequently, cells were exposed (overnight, 4°C) to anti-GLUT8 antibody, alone or in combination with antibodies against LAMP2, RAB7 and G6Pase (Supplemental Table S3). After incubation, an Alexa594-conjugated secondary antibody or an Alexa488-conjugated secondary antibody was added (1h, room temperature). Coverslips were mounted with Fluoro-Gel (Electron Microscopy Sciences – 17985-10) and DAPI (Cell signalling #4083) (Romero-Pico et al., 2018; Romero-Pico et al., 2013).

Proteomic studies

Protein identification and quantification were performed as described in previously published studies (Alvarez et al., 2019; Del Pilar Chantada-Vazquez et al., 2020; Hermida-Nogueira et al., 2020) according to following methods.

In the qualitative protein Identification, previously digested peptides of each sample were separated by Reverse Phase Chromatography in a nanoLC400 (Eksigent Technologies, Sciex) coupled to a Triple TOF 6600 mass spectrometer (Sciex) using a microflow source. Data-dependent workflow (DDA) method was used for data acquisition.

In the SWATH quantitative analysis, first it necessary the spectral library creation created using Pooles samples from each group that was run in a data dependent workflow (DDA). Only peptides with a confidence score above 99% were selected to be included in the spectral library. The SWATH acquisition method was created with 100 windows, using the Ion information from the spectral library. Then, the individual samples were analysed using a data-independent acquisition (DIA) method. The fragment ion chromatogram traces from the SWATH runs were extracted in PeakView (version 2.2) software using the SWATH Acquisition MicroApp (version 2.0) and the integrated peak areas (processed. mrkvw files from PeakView) were directly exported to the MarkerView software (Sciex) for relative quantitative analysis.

An unsupervised multivariate statistical analysis (PCA) was performed to compare the data across the samples, using, in this case, a range scale method. The average MS peak area of each protein in each sample was derived from the data of the biological replicates that were analysing by Student's *t*-test analysis (MarkerView software). This was made in order to perform a comparison among the samples based on the averaged total area of all the transitions derived for each protein. The *t*-test indicated us how well each variable distinguishes the two groups and it reported as a *p*-value. The cut off used to select the proteins were those with ap-value <0.05 and a 1.5-fold increase or decrease.

Functional analysis was performed by FunRich (Functional Enrichment analysis tool) open access software for functional enrichment and interaction network analysis (http://funrich.org/index.html).

RNA extraction, cDNA synthesis and quantitative real time PCR analysis

RNA was extracted using RNeasy Mini Spin Columns (QIAGEN, USA) according to the manufacturer's instructions. RNA concentrations of 1 µg were used for cDNA synthesis using the SensiFAST™ cDNA Synthesis Kit (BIOLINE, UK) following product protocol. Quantitative real-time PCR was performed using the QuantStudio 5 instrument (Applied Biosystems) with

TaqMan™ Gene Expression Master Mix (ThermoFisher Scientific) or SYBR green reagent (Precision ®PLUS Master Mix, PRIMER DESIGN). Specificity of the PCR amplification was considered by using negative control reactions, containing all reagents except the sample. The oligonucleotide specific primers are shown in Supplemental Table S1. Gene expression data were analysed using the ΔΔCt method, calculating the change in Ct between the gene of interest normalised against the HPRT gene and expressed as a fold change relative to the control group.

Western blotting

Total protein lysates from the liver, LX2 and THLE2 cells were subjected to SDS-PAGE and electrotransferred on a polyvinylidene fluoride membrane (Millipore). Membranes were probed with the antibodies and specific conditions described in Supplemental Table S2. Detection of proteins was performed using HRP-conjugated secondary antibodies and an enhanced chemiluminescence reagent (Thermo Scientific). Optical densities of the immunoreactive bands were measured using ImageJ software. Values were expressed relative to β-actin or α-tubulin levels. Data are expressed as a percentage of the control group.

Statistics

Results are expressed as mean ± SEM. GraphPad Prism (version 8.0) was used for the data analysis. Comparison between two groups was performed using an unpaired t-test (when parametric conditions were reached) or Mann-Whitney test (for non-parametric data). One-way ANOVA followed by Tukey's multiple comparison test (parametric) or Kruskal-Wallis test followed by Dunn's multiple comparisons test (non-parametric) were used to compare three treatments (SD, fructose, HFD). Two-way ANOVA was conducted to examine interactions between variables. For *in vitro* studies, three independent experiments were performed, each one in triplicate. Sample size and statistical values are specified in each figure legend. $P < 0.05$ was considered statistically significant.

Table S1. **Primers sequences used in the study.** Related to main Figures 2-7.

SPECIES	GENE	FORWARD 5'→3'	REVERSE 5'→3'
Mus musculus	*Abcd1*	CCTGTCTGGAGGTGAGAAGC	TGCAGCAAGTGTGTGTGGTA
	Acca	TGGGCGGGATGGTCTCTTT	AGTCGCAGAAGCAGCCCATT
	Acot2	CCCCAAGAGCATAGAAACCA	CCAATTCCAGGTCCTTTTACC
	Acox1	CAGGAAGAGCAAGGAAGTGG	CCTTTCTGGCTGATCCCATA
	Atf4	GGGTTCTGTCTTCCACTCCA	AAGCAGCAGAGTCAGGCTTTC
	Asc	TGCTTAGAGACATGGGCTTACAGG	GTCCACAAAGTGTCCTGTTCTGG
	Bip	TTCAGCCAATTATCAGCAAACTCT	TTTTCTGATGTATCCTCTTCACCAGT
	Chop	CCACCACACCTGAAAGCAGAA	AGGTGAAAGGCAGGGACTCA
	Col1a1	CCTAATGCTGCCTTTTCTGC	ATGTCCCAGCAGGATTTGAG
	Col1a2	CCGTGCTTCTCAGAACATCA	CTTGCCCCATTCATTTGTCT
	Col3	GCACAGCAGTCCAACGTAGA	TCTCCAAATGGGATCTCTGG
	Cpt1l	ATCATGTATCGCCGCAAACT	ATCTGGTAGGAGCACATGGGC
	Cpt2	CAGCACAGCATCGTACCCA	TCCCAATGCCGTTCTCAAAAT
	Cyp2b10	TGCTGTCGTTGAGCCAACC	CCACTAAACATTGGGCTTCCT
	Cyp4a14	TGACTCCAGCCTTCCACTATGA	GGCCATCAAGCTTCTCCCATTTA
	Cyp4a10	CTTCCCAAGTGCCTTTCCTAGATG	TCTGTACGCACCATTAGCCTTTG
	Elovl6	GAAAAGCAGTTCAACGAGAACG	AGATGCCGACCACCAAAGATA
	Fasn	TGGGTTCTAGCCAGCAGAGT	ACCACCAGAGACCGTTATGC
	F4-80	GCCTTCTGGATCCATTTGAA	TGCATCTAGCAATGGACAGC
	Glut2	TGTGCTGCTGGATAAATTCGCCTG	AACCATGAACCAAGGGATTGGACC
	Glut5	GGCTCAATCTTCCCCTTCATTC	ATGAATGTCTGCCCTTGG
	Hnf4a	CATGGATATGGCCGACTACAG	GCCCGAATGTCGCCATTGATCCCAGAGA
	Hprt	CAAACTTTGCTTTCCCTGGT	TCTGGCCTGTATCCAACACTTC
	Il1b	CCTGCAGCTGGAGAGTGTGG	CCAGGAAGACAGGCTTGTGC
	Il6	GATGCTACCAAACTGGATATAATC	GGTCCTTAGCCACTCCTTCTGTG
	Il15ra	CTTTCCTGGCCTGGTACATCAA	TCCATGGTTTCCACCTCAACA
	Il18	TGGCTGCCATGTCAGAAGACT	AGTTGTCTGATTCCAGGTCTCCATT
	Lclat1	TTTTATGCTCGGCCCCATTTT	CACAAGACGGCTGCTAATCCA
	Nrf2	TCAGTGACTCGGAAATGGAG	TTCACGCATAGGAGCACTGT
	Nlrp3	ACCCACAACCACAGCCTTCG	CACCCAACTGTAGGCTCTGC
	Scd1	TTCTTGCGATACACTCTGGTGC	CGGGATTGAATGTTCTTGTCGT
	a-Sma	AAACAGGAATACGACGAAG	CAGGAATGATTTGGAAAGGA
	Sult2a1	GAAGGCATACCTTTTCCTGCCAT	GTAACCAGACACAAGAATATCTCT
	Tgfb	TTGCTTCAGCTCCACAGAGA	TGGTTGTAGAGGGCAAGGAC
	Timp1	ATTCAAGGCTGTGGGAAATG	CTCAGAGTACGCCAGGGAAC
	Tnf1a	AAATGGCCTCCCTCTCATCA	AGATAGCAAATCGGCTGACG
	sXbp1	CTGAGTCCGAATCAGGTGCAG	GTCCATGGGAAGATGTTCTGG
	UsXbp1	CAGCACTCAGACTATGTGCA	GTCCATGGGAAGATGTTCTGG
	Total Xbp1	TGGCCGGGTCTGCTGAGTCCG	GTCCATGGGAAGATGTTCTGG

	FORWARD 5'→3'	PROBE 5´FAM-3´TAMRA	REVERSE 5'→3'
Glut8	CTGTCAGGGGTCAATGCTATC	GAGGCCAAGTTCAAGGACAG	GCAGTGAACAGGACCTGGAT
Hprt	TGCTGACCTGCTGGATTACATT	AGATCCATTCCTATGACTGTAG	CCCCGTTGACTGATCATTACAGTA
Afp	Mm01351346_m1 (*Applied Biosystems*)		

SPECIES	GENE	FORWARD 5'→3'	REVERSE 5'→3'
Homo sapiens	*ADAM17*	CCATGAAGTGTTCCGATAGAT	ACCTGAAGAGCTTGTTCATCG
	ASC	TGACGGATGAGCAGTACCAG	TCCTCCACCAGGTAGGACTG
	CASPASE 1	GCCTGTTCCTGTGATGTGGA	TTCACTTCCTGCCCACAGAC
	CYP4A11	ATGTCTCTGGAATCCTCCAAGCGG	ATTTCTGAATCCGTTGTAGCTCCTGG
	CYP4F2	CAACCCCACAGAGGAGGGCATGAG	GAGGCGTTGATGACAGACCG
	CYP4F3	AGGGGAGAGGAGGTTGTGTGGGACA	CAGGTGACCCAAGAACCAATTCCGTT
	GLUT8	AAGCTGAGCCTCTTGCTGTG	GGCGATTTCGGAGATGTAGA
	HPRT	CCTGGCGTCATTAGTG	TCCCATCTCCTTCATCACATC
	ICAM1	GGCCGGCCAGCTTATACAC	TAGACACTTGAGCTCGGGCA
	IL1b	CTCCGGGACTCACAGCAAAAA	GTACAAAGGACATGGAGAACACC
	IL6	GGTACATCCTCGACGGCATCT	GTGCCTCTTTGCTGCTTTCAC
	IL18	AAAGATAGCCAGCCTAGAGGTATG	GATCTATCCCCCAATTCATCCT
	NLRP3	AAGCACCTGTTGTGCAATCTGAAG	GGGAATGGCTGGTGCTCAATAC
	FASN	Hs01005622_m1 (*Applied Biosystems*)	
	HPRT	Hs02800695_m1 (*Applied Biosystems*)	

Table S2. List of antibodies used in western blotting. Related to main Figures 1, 2, 4, 5 and 7.

PRIMARY ANTIBODIES	SUPPLIER	REFERENCE	DILUTION
ACC	Cell signalling	#3662S	1:1000
B-ACTIN	SIGMA	A5316	1:5000
ATF6	Santa Cruz Biotech.	sc-166659	1:1000
ATGL	Abcam	ab109251	1.1000
BIP	Cell signalling	#3183S	1:1000
CASPASE-1	Santa Cruz Biotech.	sc-56036	1:1000
CHOP	Cell signalling	#28955S	1:1000
CPT1A	Abcam	ab128568	1:1000
pCREB	Cell signalling	#9198S	1:1000
FAS	Abcam	ab128870	1:1000
GLUT2	Santa Cruz Biotech.	sc-518022	1:1000
FGF21	Abcam	ab171941	1:1000
pIRE	Novus Biologicals	NB100-2323	1:1000
pPERCK	Cell signalling	#3179	1:1000
a-TUBULIN	SIGMA	T-5168	1:5000
SECONDARY ANTIBODIES	**SUPPLIER**	**REFERENCE**	**DILUTION**
Polyclonal rabbit anti-mouse	DAKO	P0260	1:5000
Polyclonal goat anti-rabbit	DAKO	P0448	1:5000

Table S3. List of antibodies used in immunohistochemistry and immunofluorescence. Related to main Figures 3 and 6.

PRIMARY ANTIBODIES	SUPPLIER	REFERENCE	DILUTION
GLUT8	Millipore	07-1407	1:1000 (cells)-1:500 (tissue)
G6PASE	Santa Cruz Biotech.	sc-398155	1:500
LAMP2	Santa Cruz Biotech.	sc-18822	1:200
RAB7	Santa Cruz Biotech.	sc-376362	1:500
SECONDARY ANTIBODIES	**SUPPLIER**	**REFERENCE**	**DILUTION**
Immunohistology/cytochemistry	Envision DAKO	SM-802	
Alexa Fluor 555 donkey anti-rabbit	Thermo Fisher	A 31572	1:500
Alexa Fluor 488 anti-mouse	Cell Signalling	#4408S	1:500
DAPI	Cell Signalling	#4083	1:1000

Supplemental References

Alvarez, J.V., Bravo, S.B., Garcia-Vence, M., De Castro, M.J., Luzardo, A., Colon, C., Tomatsu, S., Otero-Espinar, F.J., and Couce, M.L. (2019). Proteomic Analysis in Morquio A Cells Treated with Immobilized Enzymatic Replacement Therapy on Nanostructured Lipid Systems. Int J Mol Sci *20*.

Del Pilar Chantada-Vazquez, M., Lopez, A.C., Vence, M.G., Vazquez-Estevez, S., Acea-Nebril, B., Calatayud, D.G., Jardiel, T., Bravo, S.B., and Nunez, C. (2020). Proteomic investigation on bio-corona of Au, Ag and Fe nanoparticles for the discovery of triple negative breast cancer serum protein biomarkers. J Proteomics *212*, 103581.

Hermida-Nogueira, L., Barrachina, M.N., Izquierdo, I., Garcia-Vence, M., Lacerenza, S., Bravo, S., Castrillo, A., and Garcia, A. (2020). Proteomic analysis of extracellular vesicles derived from platelet concentrates treated with Mirasol(R) identifies biomarkers of platelet storage lesion. J Proteomics *210*, 103529.

Novelle, M.G., Vazquez, M.J., Peinado, J.R., Martinello, K.D., Lopez, M., Luckman, S.M., Tena-Sempere, M., Malagon, M.M., Nogueiras, R., and Dieguez, C. (2017). Sequential Exposure to Obesogenic Factors in Females Rats: From Physiological Changes to Lipid Metabolism in Liver and Mesenteric Adipose Tissue. Sci Rep *7*, 46194.

Porteiro, B., Fondevila, M.F., Buque, X., Gonzalez-Rellan, M.J., Fernandez, U., Mora, A., Beiroa, D., Senra, A., Gallego, R., Ferno, J.*, et al.* (2018). Pharmacological stimulation of p53 with low-dose doxorubicin ameliorates diet-induced nonalcoholic steatosis and steatohepatitis. Mol Metab *8*, 132-143.

Romero-Pico, A., Sanchez-Rebordelo, E., Imbernon, M., Gonzalez-Touceda, D., Folgueira, C., Senra, A., Ferno, J., Blouet, C., Cabrera, R., van Gestel, M.*, et al.* (2018). Melanin-Concentrating Hormone acts through hypothalamic kappa opioid system and p70S6K to stimulate acute food intake. Neuropharmacology *130*, 62-70.

Romero-Pico, A., Vazquez, M.J., Gonzalez-Touceda, D., Folgueira, C., Skibicka, K.P., Alvarez-Crespo, M., Van Gestel, M.A., Velasquez, D.A., Schwarzer, C., Herzog, H.*, et al.* (2013). Hypothalamic kappa-opioid receptor modulates the orexigenic effect of ghrelin. Neuropsychopharmacology *38*, 1296-1307.

Tuduri, E., Beiroa, D., Stegbauer, J., Ferno, J., Lopez, M., Dieguez, C., and Nogueiras, R. (2016). Acute stimulation of brain mu opioid receptors inhibits glucose-stimulated insulin secretion via sympathetic innervation. Neuropharmacology *110*, 322-332.